# Characterizing Therapeutic Vulnerabilities in Colorectal Cancer

Name: Ali Ali
Supervisor: Andrew Campbell


University of Glasgow

## Contents

## Abstract

Colorectal cancer is the global second leading cause of cancer deaths and is associated with poor prognosis. Inactivation of the gatekeeper gene APC initiates colorectal cancer and subsequent KRAS mutations confer resistance to standard anti-EGFR therapy. Cell proliferative pathways downstream of RAS such as MEK, PI3K, and mTOR further promote cancer growth, and efforts to inhibit these pathways individually demonstrated cancer resistance mechanisms by activating parallel pathways. Colorectal cancer is also heterogenous disease, which has been characterized by two transcriptomic subtyping systems: the Cell Intrinsic Transcription Signatures and the Consensus Molecular Subtypes. These subtyping systems can be utilized in clinical settings to assign patients to subtypes based on key biological features and to stratify patients into prognostic groups to predict survival and response to treatment. It was hypothesized in this research project that combination targeted treatments can alter the transcriptional landscape and aggressive subtypes of colorectal cancer to better prognosis. To address this hypothesis, genetically engineered mouse models of colorectal cancer with inactivated APC and mutated KRAS were developed and treated with two different targeted combination therapies: MEK+mTOR inhibitor AZD6244.2014 and MEK+PI3K inhibitor AZD6244.8186. The cancer cells were then RNA sequenced to generate gene expression data, which was then processed and analyzed to output the results for this project. CMSCaller R-package was used to CRIS and CMS subtype the mouse CRCs to human CRC. Galaxy software DEseq2 was used to generate the normalized differential gene expression data, and Searchlight2 was used to perform the GO hypergeometric gene set enrichment analysis and TRRUST upstream regulator analysis. Results from this analysis showed that AZD6244.2014 and AZD6244.8186 significantly downregulated transcriptional MEK signature genes and altered the transcriptomic genetic profiles associated with metabolic and immune processes. Both combination treatments also shifted the colorectal cancer subtype from an aggressive poor prognostic signature to better prognostic signatures with extended disease free survival. These results significantly demonstrate the clinical promise of targeted combination treatments in improving colorectal cancer patient survival, and should be further investigated in human whole tumor models.

## Introduction

Colorectal cancer (CRC) is a malignancy whose mortality has declined progressively in the past decades [1, 2]. This is primarily contributed to broader implementation of early detection screening programs, improved prevention measures, and the development targeted systemic therapies [1-3]. However, CRC remains the second most common cause of cancer deaths and the third most commonly diagnosed malignancy worldwide [1-3]. Furthermore, patients diagnosed with CRC have a poor prognosis of 64% 5-year survival, and if the cancer metastasizes, it results in a dismal 12% 5-year survival [3, 5]. This emphasizes the demand for not only a better understanding of the disease but also for improved targeted treatments that promise higher survival rates. CRC is also a highly heterogenous disease with a diverse landscape of genetic mutations, immune profiles, stromal components, and clinical outcomes, which has long complicated disease characterization and treatment options [1, 2, 6, 7].

In colorectal carcinogenesis, there are three partnering driver genes whose alterations sequentially lead to cancer progression [7, 8]. Adenomatous polyposis coli (APC) is the earliest gene to be inactivated in CRC and is the most frequently mutated gene in this disease [4, 7, 8]. APC is a tumor suppressor and considered the gatekeeper gene in CRC due to its role as an antagonist to WNT signaling [7, 8]. Inactivation of APC results in overactivation of the WNT cascade, leading to uncontrolled cell proliferation and adenoma formation [7, 8]. Mutations in the oncogene KRAS typically follow APC inactivation and further promote adenoma growth [1, 5, 8]. RAS serves as a signaling node downstream of epidermal factor growth receptors (EGFRs) to activate mitogen-activated protein kinase (MAPK) pathways, and therefore, mutations in KRAS lead to the constitutive activation of EGFRs and downstream pathways [5, 8-10]. This then confers cancer resistance to EGFR inhibitors such as cetuximab and limits the available treatment options [2, 5, 8-10]. In the late events of colorectal carcinogenesis, inactivation of tumor suppressor TP53 transitions adenomas to carcinomas and disrupts TP53 functions such cell cycle regulation [1, 2, 11].

Such alterations in tumor suppressors and oncogenes lead to aberrant cell proliferative signaling stimulated by three frequently deregulated pathways in CRC: mitogen-activated extracellular signal-regulated kinase (MEK) [10, 12, 13], phosphoinositide 3-kinase (PI3K) [14-16], and mechanistic

target of rapamycin (mTOR) [17-19] (**figure 1**). These are well-characterized canonical pathways downstream of RAS, and are involved in CRC progression and oncogenic behavior. The MEK pathway is a subfamily of the MAPK pathway and is one of the most important cascades in cell proliferation [10, 12, 13]. Once activated, MEK drives cell cycle progression and proliferation and inhibits apoptosis [10, 12, 13]. Targeting the MEK pathway by the MEK inhibitor AZD6244 has been shown to reduce cancer cell proliferation and drive apoptotic signaling [12, 13]. The PI3K pathway is another commonly mutated pathway, and its activation stimulates AKT leading to downstream signaling events that promote cancer cell growth and survival [14-16]. Targeting the PI3K pathway by p110/PI3K inhibitor AZD8186 has been demonstrated inhibit these cancer promoting effects [14, 15]. The mTOR pathway also plays a critical role in regulating cell proliferation in CRC by deregulating key metabolic processes and cellular energy [17-19]. When activated, mTOR triggers downstream proteins that stimulate cellular growth and modulate metabolism and lipid synthesis [17-19]. Targeting the mTOR pathway by next generation mTOR inhibitor AZD2014 has also been shown to suppress cancer cell proliferation and can potentially block the modulation of normal metabolic processes [18]. Despite the promise of these inhibitors, their use as monotherapies has demonstrated that cancers develop resistance mechanisms by activating other parallel pathways to maintain cell growth, and hence their use as combination treatments should be investigated in CRC [16, 17, 19].

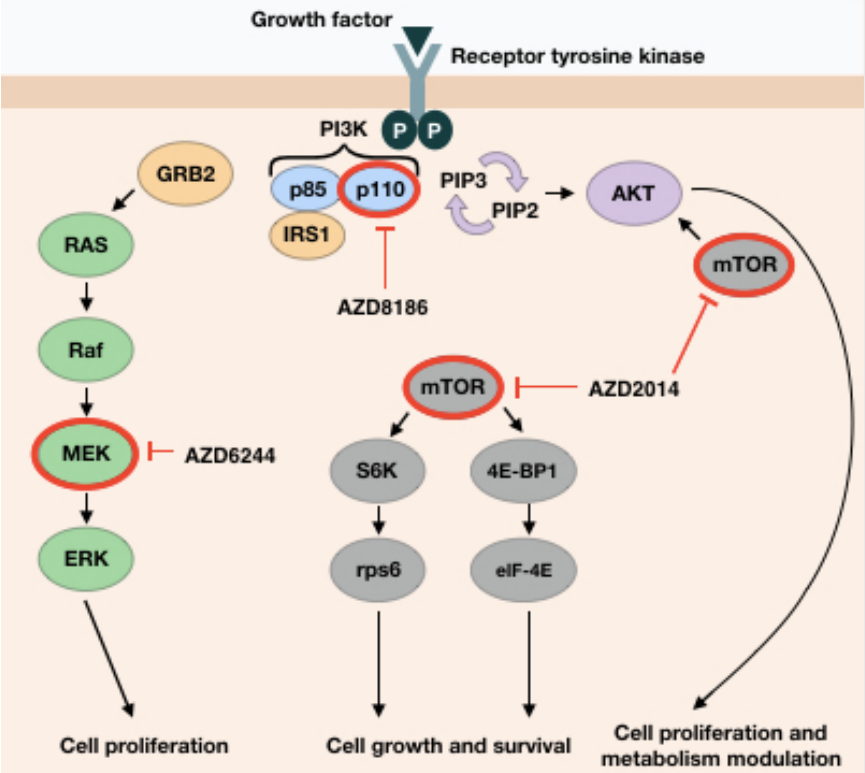


**Figure 1 | Commonly Mutated Pathways in CRC and Their Inhibitors.** Three canonical pathways downstream of RAS are frequently dysregulated in CRC and consequently promote cancer cell growth: MEK is a key proliferative pathway, and its overactivation results in uncontrolled cell division and reduced apoptotic signaling, which can be inhibited by AZD6244; PI3K is also commonly mutated in CRC, and its hyperstimulation maintains cancer cell survival, which can be suppressed by the p110/PI3KB inhibitor AZD8186; mTOR is another often deregulated pathway, and its overactivation elicits cancer cell proliferation by modulating normal cell metabolism, which can be suppressed by the next generation mTOR inhibitor AZD2014.

Given the biological heterogeneity, driver gene alterations, and commonly mutated pathways of this disease, efforts to characterize and subtype CRC have improved our understanding of this disease and its therapeutic approaches [2, 20-22]. Such efforts have come through robust transcriptomic analyses of large scale CRC patient data sets, leading to two subtype classification systems. The Cell Intrinsic Transcription Signatures (CRIS) system is based on CRC cell-specific characteristics, excluding the stroma, and it clusters the disease into 5 signature subsets - CRIS-A, B, C, D, and E- with each signature having unique cell-intrinsic gene expression traits and clinical outcomes [20] (**table 1.1**). The Consensus Molecular Subtypes (CMS) system is based on the analysis of whole CRC tumors, including the stroma, and it clusters the disease into 4 subtypes - CMS1, 2, 3, and 4 - with each subtype having characteristic genomic, mutational, stromal, and immune profiles [21, 22] (**table 1.2**). In clinical settings, CRIS and CMS can be utilized not only to stratify patients into prognostic groups to predict survival and response to treatment

but also to predict CRC clinical behavior based on subtype-specific tumor phenotype [2, 20-22]. Furthermore, in pre-clinical settings, subtyping mouse CRC can cross-compare biological characterization and clinical outcomes to human CRC [23, 24].

| Table 1.1. | CRIS-A | CRIS-B | CRIS-C | CRIS-D | CRIS-E |
|---|---|---|---|---|---|
| MOLECULAR FEATURES | MSS CIN-Low KRAS $^{mut}$ | No Enriched Features | CIN-High TP53 $^{mut}$ MYC Amplified | CIN-High IGF2 Amplified | CIN-High KRAS $^{mut}$ TP53 $^{mut}$ |
| PATHWAYS | Glycolysis Inflammation MSI-like Mucinous | EMT High TGFβ High | EGFR High ERBB3 High | IGFR High FGFR High WNT High LGR5$^{+}$ like | WNT High Paneth Cell-like |
| OUTCOME | + | - | + | + + | + |
| THERAPY RESPONSE | Cetuximab No Response | | Cetuximab Response | Cetuximab No Response | Cetuximab No Response |

| Table 1.2. | CMS1 | CMS2 | CMS3 | CMS4 |
|---|---|---|---|---|
| MOLECULAR FEATURES | MSI-High CIMP-High BRAF $^{V600E}$ | CIN-High TP53 $^{mut}$ | CIN-Intermediate CIMP-Low KRAS $^{mut}$ | CIN-High |
| PATHWAYS | Immune Response JAK-STAT High | WNT High MYC High SRC High | Metabolic Dysregulation | EMT High TGFβ High Matrix Remodeling |
| STROMA | Immune Cells | | | Desmoplasia Fibroplasia |
| OUTCOME I-III / IV | + + / - - | + / + | + / - | - / - |
| THERAPY RESPONSE | 5-FU No Response Immunotherapy Response | FOLFOX Response Cetuximab Response | FOLFOX Response | FOLFOX No Response FOLFIRI No Response Cetuximab No Response |

**Table 1.1-1.2 | The Biological and Clinical Characterization of CRC Subtypes: CRIS and CMS.** CRC heterogeneity has been characterized by two robust transcriptomic subtype classification systems - CRIS and CMS. CRIS and CMS can be clinically utilized to stratify patients into prognostic groups to predict survival and response to treatment, and can be used to predict CRC clinical behavior based on subtype-specific biological features. **1.1.** CRIS is based on CRC cell-specific characteristics, excluding the stroma, and it clusters the disease into 5 signature subsets - CRIS-A, B, C, D, and E -, each described in terms of cell-intrinsic molecular features, activated pathways, and clinical outcomes. **1.2.** CMS is based on whole CRC tumor characterization, including the stroma, and it clusters the disease into 4 subtypes - CMS1, 2, 3, and 4 -, each with distinctive molecular features, activated pathways, and clinical outcomes as well. CIMP, CpG island methylator phenotype; CIN, chromosomal instability; EMT, epithelial to mesenchymal transition; MSI, microsatellite instability; MSS, microsatellite stability; 5FU, Fluorouracil.

With such advances in our understanding of CRC, along with the recognition that cancers evolve under pressure from treatment, an important question is posed: can combination targeted treatments approaches modulate the transcriptional landscape and aggressive subtypes of CRC to better prognostic signatures?

To address this question, preliminary data has been processed and analyzed in this research. The preliminary data is raw gene expression data generated by RNA sequencing genetically engineered mouse models of aggressive CRCs treated with combination treatments and drug vehicle for control. The treated and control groups were in replicates of four. The genetically engineered mouse model used was the APC KRAS (AK) mutated CRC model, which is a robust, tractable mouse model that enables the study of the phenotypic impact of common CRC associated gene alterations in-vivo. The model was created by the transgenic expression of tamoxifen-inducible Cre recombinase under the control of Villin promoter, which is exclusively expressed in mouse intestinal epithelial cell. The transgene is then used to delete APC and express a mutant copy of KRAS, hence creating the AK model. As part of the preliminary data, the cell proliferative effects of deleting APC and mutating KRAS in the mouse intestinal epithelium were evaluated. APC deletion and KRAS mutation alone had minor proliferative effects compared to the wild type, whereas simultaneous APC deletion and KRAS mutation demonstrated exacerbated hyperproliferation (**figure 2A**). The treatments used in this project were the combination treatments AZD6244.2014 and AZD6244.8186. Drug vehicle treatments were used to control for treatment. Combination treatments of the pathway inhibitors were used in this project as the monotherapies on their own are ineffective in suppressing the hyperproliferative effects of the AK model. Cancers develop resistance mechanisms against the monotherapies by activating parallel pathways to maintain cell growth, and hence combination treatments can block these parallel pathways of resistance [16, 17, 19]. This has been validated by measuring the anti-proliferative effects exerted by the treatments on AK CRCs, and it was clear that the combination treatments had effectively suppressed the hyperproliferative effects of AK CRC compared to the monotherapies **(figure 2B**).

**Figure 2 | Hyperproliferation in the AK CRC Model and Its Effective Suppression by AZD6244.2014 and AZD6244.8186.**

**(A)** The proliferative effects of deleting APC, mutating KRAS, or both in mouse intestinal epithelial cells was measured using BrdU staining. Compared to the WT, which showed little proliferation, the APC deficient cells were twice as proliferative and KRAS mutated cells were just as mildly proliferative. The double APC KRAS mutated cells were the most proliferative with four fold the BrdU positivity of the WT. **(B)** The anti-proliferative effects of targeted monotherapies and combination treatments in APC KRAS mutated epithelial intestinal cells was measured using BrdU staining. Compared to the vehicle-treated group, the monotherapies (AZD6244, AZD8186, and AZD2014) demonstrated little change in the suppression of proliferation while the combination treatments (AZD6244.2014 and AZD6244.8186) showed a more effective inhibition of cell proliferation.

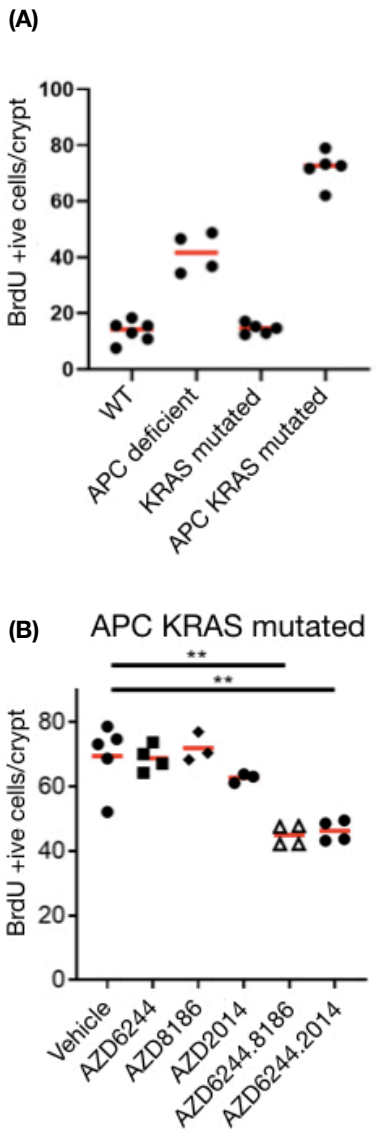


## Hypothesis

Targeted combination treatments can alter the transcriptional landscape and aggressive subtypes of CRC to better prognosis.

## Aims

1. to determine how effective the combination treatments inhibit the target pathways in AK CRC.
2. to identify the genetic programs responsible for the therapeutic effect.
3. to determine if the efficacious treatments alter transcriptomic signatures in the AK CRC.
4. to identify human patient populations which may benefit from these efficacious treatments.

## Pilot Data

### AZD6244.2014 and AZD6244.8186 Effectively Downregulate Transcriptional MEK Signature Genes in AK CRC

This set of results shows the differential gene expression of transcriptional MEK pathway signature genes in AK CRC mouse models treated with AZD6244.2014 or AZD6244.8186 compared to drug vehicle-treated controls. Transcriptional MEK signature genes are a set of genes known to be impacted by AZD6244-mediated inhibition of the MEK pathway as demonstrated by Dry et al [25]. Since MEK is the key proliferative signaling cascade controlling CRC cell growth [10, 12, 13] and is targeted by both combination treatments, an effective significant downregulation of the transcriptional MEK genes can demonstrate effective inhibition of the key cell proliferative pathway in AK CRC by the combination treatments.

Differential gene expression analysis of the transcriptional MEK genes showed effective and significant downregulation of 16 MEK genes by AZD6244.2014 and AZD6244.8186 ($P.adj<0.05$) (**figure 3**). The log2fold change was comparable in both treatment groups, but AZD6244.8186 showed more effective downregulation of 5 MEK genes: CLU, ETV4, ETV5, GDF15, and S100A6. A possible explanation is the PI3K-dependent regulation of those 5 genes [26-32], and hence the presence of a PI3K inhibitor in AZD6244.8186 has most likely amplified their downregulation. An upregulation of 4 MEK genes was also observed in both combination treatment groups, which could be attributed to compensatory transcriptional upregulation in response to MEK inhibition. When the same differential gene analysis was performed on mTOR and PI3K signature genes for AZD6244.2014 and AZD6244.8186 respectively, there were not enough downregulated differential genes to conclude significant transcriptional inhibition of these pathways. It is plausible that the inhibition of these pathways may not have been transcriptionally driven, and rather a knock-on effect on their target cellular processes may have occurred.

Overall, the significant downregulation of the transcriptional MEK gene signatures by AZD6244.2014 and AZD6244.8186 indicate the effective suppression of the key cancer cell proliferative pathway, and further highlight the efficacy of the combination treatments.

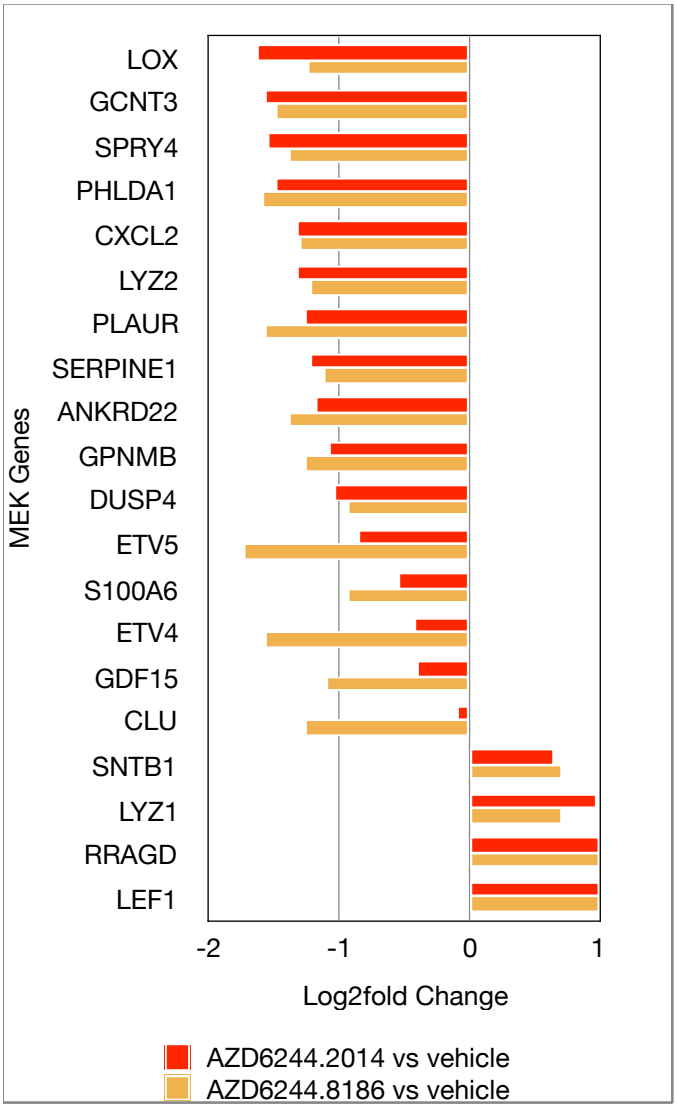


**Figure 3 | AZD6244.2014 and AZD6244.8186 Significantly Downregulate Transcriptional MEK Signature Genes in AK CRC.** A set of genes shown to be transcriptionally suppressed by AZD6244-mediated MEK inhibition was run across the significant differential genes of each of the combination treatments vs vehicle, which showed significant and effective downregulation of 16 MEK genes. AZD6244.8186 showed higher downregulation than AZD6244.2014 in 5 of the MEK genes, which may be associated with their PI3K-dependent regulation, and hence PI3K inhibition by AZD6244.8186 amplified their downregulation. An upregulation of 4 MEK genes was also observed in both combination treatments, possibly as a compensatory upregulation to MEK inhibition. P.adj<0.05, n =4.

To generate the differential gene expression data for AZD6244.2014 and AZD6244.8186 vs vehicle-treated controls, the raw gene expression data was fed into Galaxy DEseq2 [33]. In the analysis, the thresholds for significant differential genes were P.adj and absolute log2fold change values of 0.05 and 1.0 respectively. To generate the differential gene expression of the transcriptional MEK genes, a list of genes associated with transcriptional MEK pathway signature genes from Dry et al [25]. was run across the differential gene expression data of AZD6244.2014 vs vehicle and AZD6244.8186 vs vehicle.

### AZD6244.2014 and AZD6244.8186 Modulate Metabolic and Immune Gene Profiles in AK CRC

This set of results shows GO Hypergeometric Gene Set Enrichment Analysis (HGSEA) and Upstream Regulator analysis (UREG) of AK CRC mouse models treated with AZD6244.2014 or AZD6244.8186 compared to the drug vehicle-treated controls. HGSEA can identify the genetic and biological pathways behind the response to treatment, and UREG can then help determine the transcriptional regulators controlling the differential biology impacted by the treatments [33]. Hence, by analyzing and determining the highest enriched gene sets and upstream regulators, the genetic mechanisms and the underlying phenotypes by which the combination treatments may have driven response can be identified.

HGSEA of the AZD6244.2014 vs vehicle-treated mouse models was performed and then the significant gene sets were sorted by highest log2fold enrichment (P.BH<0.05, log2fold enrichment>1). The highest enriched upregulated gene sets were metabolic and the highest enriched downregulated gene sets were mainly immune signatures associated with immune cell migration and chemotaxis (**appendix figure S1A**). The same analysis for AZD6244.8186 vs vehicle-treated models showed that the highest enriched upregulated gene sets were diverse metabolic signatures or associated with lipid/sterol biosynthesis and transport, and the highest enriched downregulated gene sets were immune signatures similar to those of AZD6244.2014 (**appendix figure S1B**). To determine the extent of enrichment of metabolic and immune gene sets compared to other gene sets, the proportion of metabolic and immune enriched gene sets to all other enriched gene sets and the number of significant differentially expressed genes (SDEGs) (P.adj<0.05, absolute log2fold change>1) controlling these gene sets were analyzed. The analysis revealed that for AZD6244.2014, the enriched gene sets were: 6% metabolic (37 SDEGs), 3% lipid/sterol biosynthesis and metabolism (12 SDEGs), 2% reactive oxygen species (ROS)-associated (12 SDEGs), and 23% immune (51 SDEGs) (**appendix figure S1C**). As for AZD6244.2014, the enriched gene sets were: 9% metabolic (120 SDEGs), 3% lipid/sterol biosynthesis and metabolism (55 SDEGs), 1% ROS-associated (24 SDEGs), and 16% immune (83 SDEGs).

To specify the metabolic and immune processes most influenced by the treatments, the enriched gene sets associated with metabolism and immune processes were extracted and sorted by highest log2fold enrichment. The results revealed that the highest enriched metabolic gene sets for AZD6244.2014 were diverse but more associated with lipid, hormone, and nucleotide metabolism (**figure 4A**), and AZD6244.8186 were diverse as well but more related to glutathione, retinoic acid, and nitric oxide metabolism (**figure 4B**). The highest enriched immune gene sets were largely immune cell chemotaxis and chemokine signaling for both treatments (**figure 4C, D**).

**(A)**

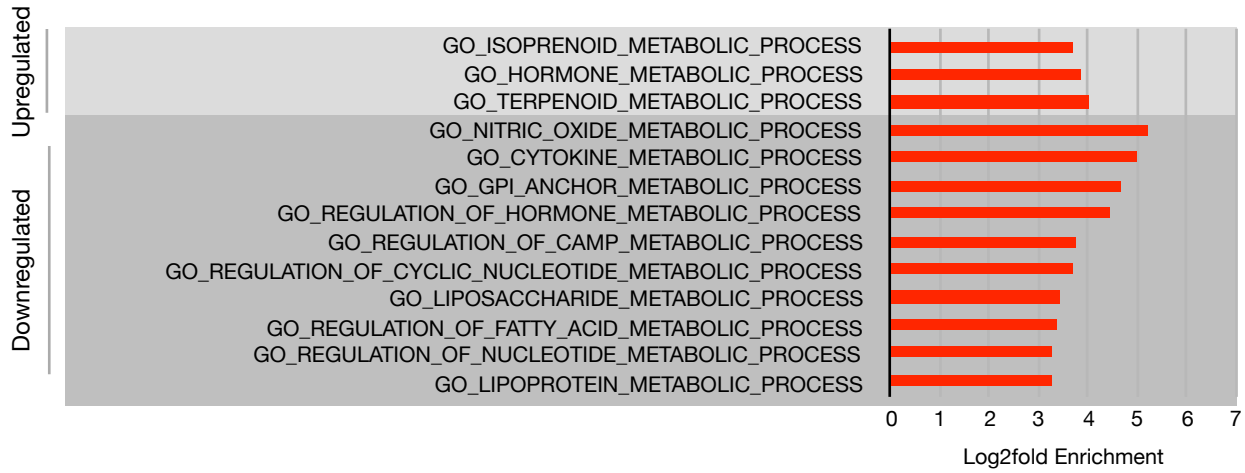


**(B)**

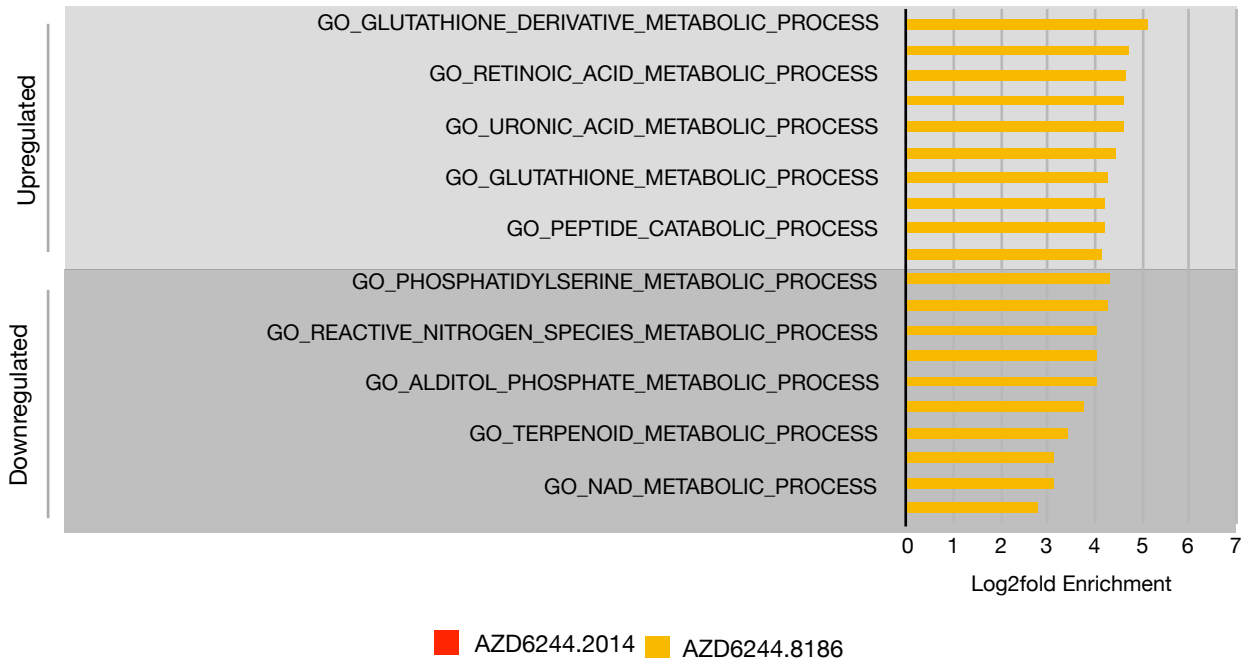

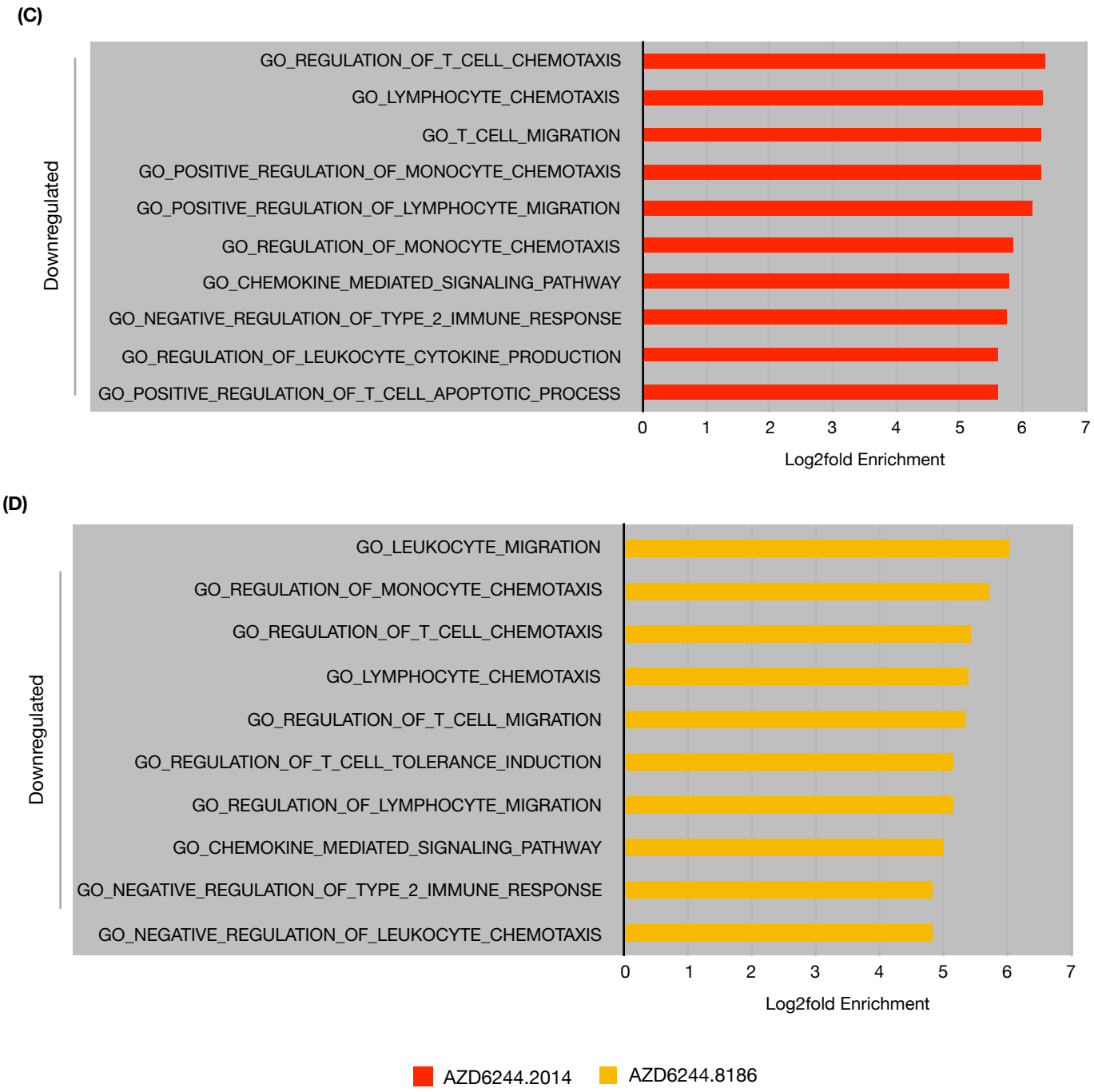


**Figure 4 | The Highest Enriched Metabolic and Immune Signature Gene Sets by AZD6244.2014 and AZD6244.8186 Treatment in AK CRC. (A)** the highest enriched metabolic gene sets (upregulated and downregulated) for AZD6244.2014 were heterogenous but more associated with lipid, hormone, and nucleotide metabolism. **(B)** the highest enriched metabolic gene sets (upregulated and downregulated) for AZD6244.8186 were diverse as well but more related to glutathione, retinoic acid, and nitric oxide metabolism. **(C) (D)** the highest enriched immune gene sets (upregulated and downregulated) for AZD6244.2014 (red) and AZD6244.8186 (yellow) were largely immune cell migration and chemokine signaling for both treatments. Enrichment P.BH<0.05, n=4

To further specify the metabolic and immune processes most influenced by the treatments on the individual gene level, the SDEGs (P.adj<0.05, absolute log2fold change>1) associated with the enriched metabolic and immune profiles were analyzed (**figure 5**). Downregulated metabolic genes included ones typically overexpressed in cancers: HK2 controls catalysis in glycolytic metabolism implicated in the tumorigenic Warburg aerobic glycolysis [34-38]; CYP1B1 controls metabolism of drugs, lipids/cholesterol, and potential carcinogens [39, 40]. As for upregulated metabolic genes: GSTK1 and GSTT1 are glutathione transferase enzymes that function in metabolic cellular detoxification [41, 42]; ADH7 and ALDH1A1 control catalysis of alcohol and aldehydes [43, 44]; RDH5 and LRAT control retinol metabolism [45, 46]. Oncogenic ROS associated genes were also significantly downregulated: DUOXA2, a producer of $H_2O_2$ in the colon [47, 48]; HIF3A, a mediator of hypoxia signaling through STAT3 phosphorylation [49, 50]; NOS2, an inflammation responsive enzyme influencing cell redox states [51-53]. Furthermore, key immune-related genes in tumorigenesis were downregulated: ADAM8, a mediator of cell migration associated with various malignancies including CRC [54-56]; ANXA1, a regulator of hydrodynamic stress in CRC that promotes metastatic potential [57-59]; CCL2-CCR2, CXCL13-CXCR5, and CCL20, immune cell chemotactic axises implicated in CRC metastasis [60-62]. As for upregulated immune associated genes: LECT2, a chemotactic factor downstream of WNT cascade with a tumor suppressor role in CRC [63].

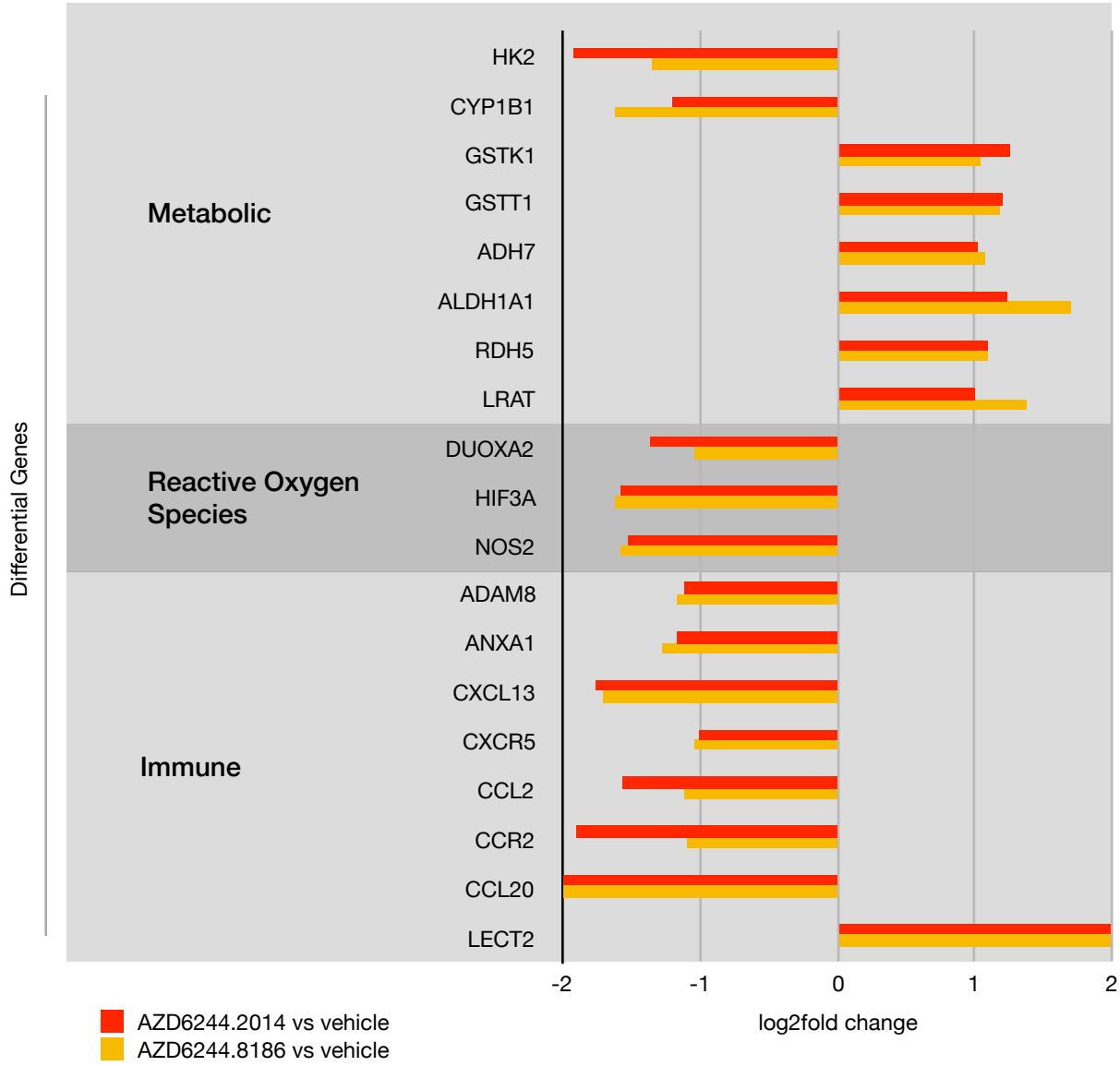


**Figure 5 | AZD6244.2014 and AZD6244.8186 Significantly Impact Genes Associated With Key Tumorigenic Metabolic and Immune Processes.** The combination treatments significantly downregulated oncogenic metabolic genes controlling Warburg glycolytic metabolism and carcinogens metabolism, and upregulated metabolic genes associated with glutathione, alcohol, aldehydes, and retinol metabolism. Furthermore, the combination treatments also downregulated ROS associated genes involved in $H_2O_2$ production and hypoxia signaling. And as for immune-related genes, the combination treatments downregulated genes that potentially lead to metastasis through the regulation of hydrodynamic stress or immune cell chemotaxis, and upregulated genes that function as chemotactic factors and tumor suppressors against WNT signaling. P.adj<0.05, n=4

Finally, to determine the upstream regulators and transcription factors controlling the enrichment of the gene sets gene sets, UREG of the significantly activated/inhibited upstream regulators (P.BH enrichment<0.05, absolute activation z-score>2) for AZD6244.2014 vs vehicle and AZD6244.8186 vs vehicle-treated models (**figure 6**) showed that both combination treatments significantly deactivated REL, RELA, IKBKB, and NFKB1, which are subunits of the transcription factor NFKB that regulates many cellular processes including ROS, glycolytic metabolism, and cytokine-driven immune responses [64-69]. NFKB1 was the highest deactivated upstream regulator for both combination treatments (**appendix figure S2**). Other upstream regulators significantly deactivated by both AZD6244.2014 and AZD6244.8186 include STAT3, STAT6, and JUN, which are cancer growth-promoting transcription factors downstream of the targeted pathways. Additionally, STAT3 and STAT6 regulate an immune process associate with T-helper cell differentiation [70-72]. POU2F2 is also mutually targeted by the combination treatments, and is a common transcription factor binding site in immunoglobulin gene promoters [73, 74]. As for the uniquely deactivated upstream regulator per treatment, AZD6244.2014 significantly deactivated SPI1, AR, and NR1I3, which regulates the expression of cytochrome P450 family members involved in drug metabolism [75]. AZD6244.8186 significantly deactivated a wider range of upstream regulators that include ATF2, known for its oncogenic role in aggressive RAS-mutated cancers [76], CEBPA, a key regulator of glucose and lipid metabolism [77], SMARCA4, APEX1, PAX3, NCOA3, EGR1, NFE2, and SPIC.

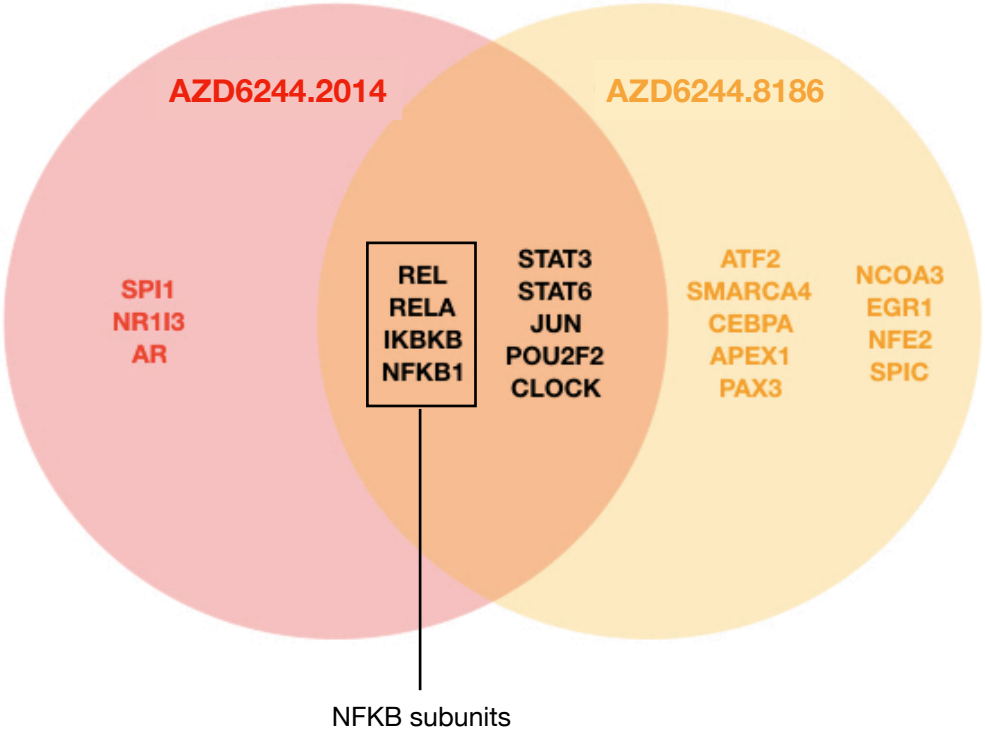


**Figure 6 | AZD6244.2014 and AZD6244.8186 significantly deactivate upstream regulators associated with metabolism and immune process in AK CRC.** UREG of AZD6244.2014 vs vehicle and AZD6244.8186 vs vehicle showed that both combination treatments mutually deactivate upstream regulators associated with different metabolic and immune processes: subunits of NFKB - NFKB1, REL, RELA, IKBKB - are implicated in promoting the oncogenic Warburg metabolic switch and different immune functions; STAT3 and STAT6 regulate T-helper cells differentiation; POU2F2 serves as a binding site in immunoglobulin gene promoters. Upstream regulators deactivated only by AZD6244.2014 include SPI1, AR, and NR1I3, a regulator of drug metabolizing genes. Upstream regulators deactivated only by AZD6244.8186 include a wider range of regulators: ATF2, an oncogene in RAS-mutated cancers, CEBPA, a key metabolic regulator, SMARCA4, APEX1, PAX3, NCOA3, EGR1, NFE2, and SPIC. Enrichment P.BH<0.05, n=4.

All together, AZD6244.2014 and AZD6244.8186 significantly modulate metabolic and immune profiles in AK CRC mouse models compared the vehicle-treated models by highly enriching gene sets associated with these profiles. The SDEGs and the upstream regulators - particularly NFKB subunits - impacted by the combination treatments regulate key metabolic and immune signaling processes that are critical in cancer progression. In other words, these results indicate an

underlying metabolic phenotype with a suppressed immune cellular chemokine signaling driving the effect of the treatments. It is important to note that the enriched downregulation of immune cell migration and chemotaxis does not mean that the treatments are driving an immune phenotype but are rather driving an epithelial expression of immune related chemokines/ cytokines.

To generate the HGSEA and UREG data, the differential gene expression data was fed into Searchlight2 [33], a software for visualizing results from omic datasets. Searchlight2 performs HGSEA by filtering the GO biological processes database to include only genes that were also in both the differential gene expression file and the background file. For each set of candidate genes, the number of overlapping genes with each gene set in the database is determined. A hypergeometric test is then performed for each candidate set and gene set combination using the number of genes in the expression set as the background size. To correct for multisampling, Searchlight2 applies a Benjamini-Hochberg correction. The thresholds for significant gene sets are adjusted P-value and absolute log2fold change of 0.05 and 0.0 respectively. As for UREG, Searchlight2 performs the same function in the TRRUST database for upstream regulators. The thresholds for significant upstream regulators are adjusted P-value, absolute log2fold enrichment, and absolute activation z-score of 0.05, 0.0, and 2.0 respectively.

### AZD6244.2014 and AZD6244.8186 Shift CRIS Subtype of AK CRC to Better Prognostic Subtypes

This final set of results show the CRIS and CMS subtypes of the AK CRC mouse models treated with AZD6244.2014, AZD6244.8186, or drug vehicle. Since every CRIS and CMS subtype is characterized by distinctive gene traits and clinical outcomes [2, 20-22], subtyping the drug combination-treated and control-treated models will not only identify the change in biological characterization of the cancers associated with therapy but will also determine the prognostic value offered by the combination treatments. In this way, a shift from a poor prognostic subtype to a better prognostic subtype will signify response to treatment. Furthermore, subtyping the mouse models to human CRC will relate the results to human patient population. Hence, the results in this section will determine if the combination treatments alter the transcriptomic subtype

signatures in the AK CRC model and will identify human patient populations which may benefit from these treatments

CMS subtyping of the vehicle-treated mouse models revealed a strong correlation to CMS4, which is characterized by mesenchymal and stromally invasive tumors with high TGFβ activation [21] (**figure 7**). Surprisingly, the AZD6244.2014 and AZD6244.8186 treated models remained strongly expressive of CMS4 as well. While in CRIS subtyping, the vehicle-treated mouse models showed a strong correlation to CRIS-B, which identifies cancers with high cellular TGFβ signaling and epithelial to mesenchymal transition [20]. In terms of clinical outcome, CRIS-B is associated with poor prognosis [20]. As for the AZD6244.2014-treated models, the CRIS subtype shifted to CRIS-D, which represents cancers marked by amplified IGF2, high IGFR, FGFR, and WNT signaling, and good prognostic outcomes [20]. Also for the AZD6244.8186 treated models, the CRIS subtype shifted to CRIS-E, which is characterized by Paneth cell-like cancers with high WNT signaling and a good clinical outcome [20]. To further understand the prognostic value of the CRIS subtypes, the Kaplan Meier graph from Isella et al. represents disease free survival (DFS) of CRIS subtypes from a CRC gene expression data set. The survival graph reveals that CRIS-B is associated with the worst DFS among CRIS subtypes, while CRIS-D and CRIS-E have the two highest DFS [20]. Hence, AZD6244.2014 and AZD6244.8186 have taken AK CRC from the worst prognostic signature to the best two prognostic signatures.

There is a caveat to CMS subtyping in this model of CRC. Ideally, CMS subtyping by CMSCaller involves characterization of whole tumors, which includes cancer cell and stromal traits [21, 23]. In other words, CMS subtyping requires the presence of a stroma for accurate characterization. The CRC model used in this project, however, is not a whole tumor but transformed mouse intestinal epithelium cells without a stromal component. Hence, the CMS stromal-based characterization would be inaccurate in a model with no stroma. CRIS, on the other hand, is defined more by cell-specific and epithelial characterizations rather than stromal ones, and hence are more relevant for the analysis in this project.

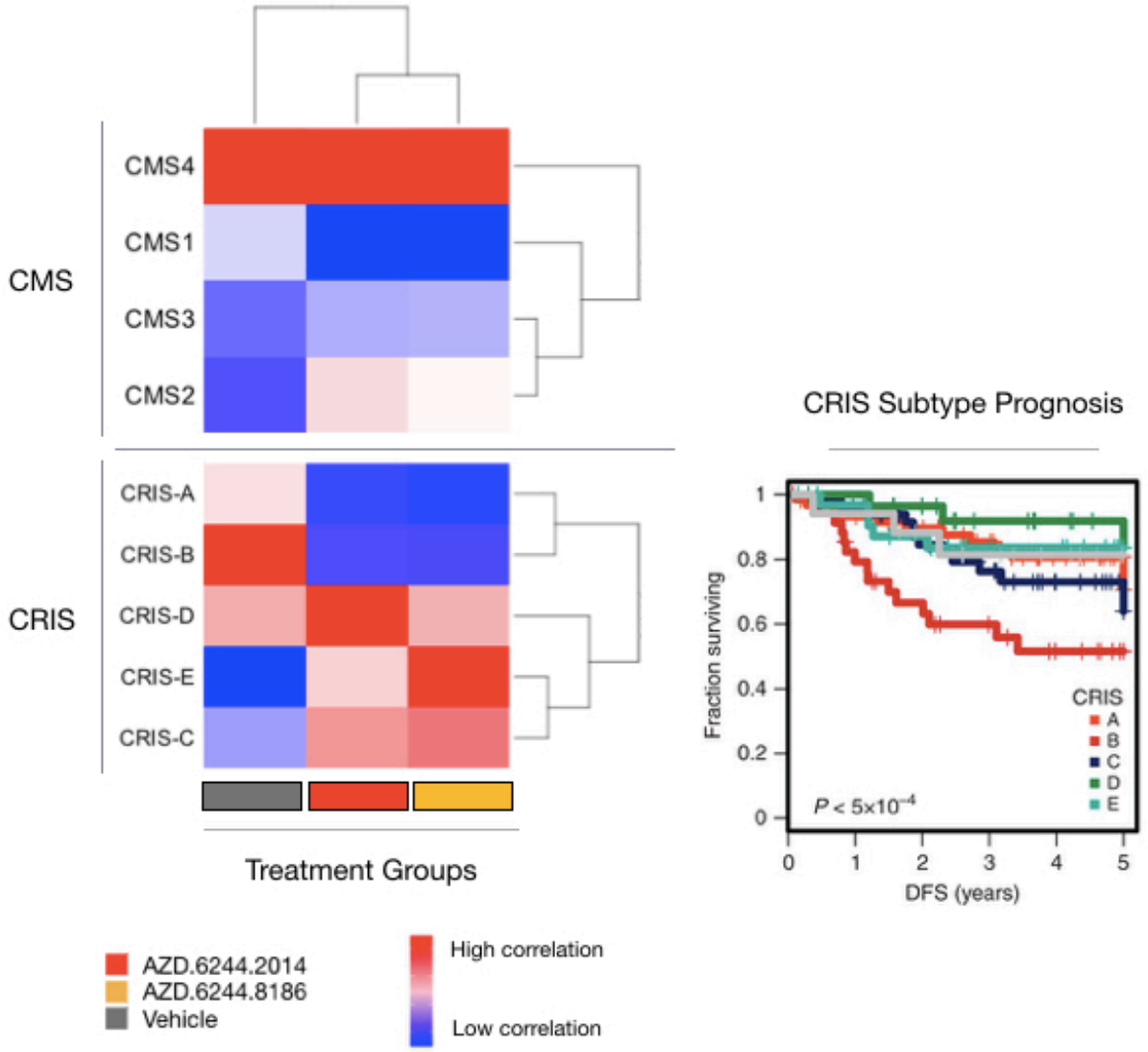


**Figure 7 | AZD6244.2014 and AZD6244.8186 Shift CRIS Subtype of AK CRC to Better Prognostic Subtypes.** In CMS subtype analysis, the vehicle-treated mouse models had a high correlation to CMS4, which is characterized by mesenchymal and stromally invasive tumors with high TGFβ activation. The combination treated groups remained highly expressive of CMS4. In CRIS subtype analysis, the vehicle-treated mouse models had a strong CRIS-B correlation, which identifies poor prognostic cancers with high cellular TGFβ signaling and epithelial to mesenchymal transition. AZD6244.2014 treatment shifted the subtype to CRIS-D, which are better prognostic cancers with high IGF2, high IGFR, FGFR, and WNT signaling. AZD6244.8186 treatment shifted the subtype to CRIS-E, which are also better prognostic cancers that are Paneth cell-like and WNT-high. The Kaplan Meier plot shows the prognosis of CRIS-subtypes in terms of disease free survival (DFS), and it demonstrates how the combination treatments shifted the AK CRC from the worst prognosis to the best two prognostic signature subtypes. n=4.

*Isella, C., Brundu, F., Bellomo, S. et al. Nat Commun 8, 15107 (2017).*

Taken together, the results collectively demonstrate that AZD6244.2014 and AZD6244.8186 shift the CRIS subtype of AK CRC from the worst DFS outcome to the best two prognostic subtypes. The combination treatments shifted the CRIS signature away from a characteristically invasive cancer subtype, thereby demonstrating the promise of suppressing potential epithelial to mesenchymal transitions. The combination treatments also shifted the CRIS subtype away from a signature marked by high cellular TGFβ signaling, which possibly signifies that the treatments may have a role in suppressing TGFβ activity in CRC cells. This major transcriptional switch to better prognostic subtypes in the treated groups indicates that the cancers have positively responded to AZD6244.2014 and AZD6244.8186, and that the combination treatments have the potential to extend DSF of patients with aggressive AK CRIS-D CRCs. While no shift in CMS subtype was observed as a result of the combination treatments, it was due to the inconsistency of using a stromal-based subtyping system in a cancer model that lacks a stroma.

The CMS and CRIS subtyping results were generated using the R-package CMSCaller [23]. The preliminary raw gene expression data along with human Entrez IDs were first inputted into R to replace the ENSEMBLE gene IDs in the expression data with the equivalent human Entrez IDs since CMSCaller recognizes the latter. CMSCaller was then used to perform the CRIS and CMS subtyping of each of the four replicates in treated and control groups present in the gene expression data by calculating a distance value to each CRIS and CMS subtype. Finally, the heat map was created using the average CRIS and CMS subtyping distance value for each treatment and control group.

## Further Lines of Investigation

### AK CRC Cell/Tumor Mouse Model

The genetically engineered tumor model of AK CRC can be used to determine the influence of the microenvironment on the therapeutic response to AZD6244.2014 and AZD6244.8186. Furthermore, The tumor model can be utilized to validate the CMS subtyping results since the classification system requires the presence of a stroma in the model. The genetically engineered AK CRC mouse models will be divided into three groups: AZD6244.2014-treated, AZD6244.8186-treated, and drug vehicle-treated. Drug vehicle treatment will be used as control for combination therapy treatment.

**Ethics statement**: mouse experiments will be performed in accordance with a granted UK Home Office license and ARRIVE guidelines and will be reviewed by the animal welfare and ethical review board of the University of Glasgow.

**Tumor generation**: in-situ CRISPR-Cas9-based editing of APC will be performed in colon epithelial cells followed by orthotopic transplantation of the APC-edited colon organoid to generate the AK CRC mouse model. First, APC will be deleted through a colonoscopy-guided mucosal injection of a Cre (PGK) lentivirus into the colon mucosa of $APC^{fl/fl}$ mice. Then, Cre recombinase driven by the Villin (epithelial-specific) and Lgr5 (intestinal stem cell-specific) promoters will be activated and Cas9 will be expressed by the mucosal delivery of low dose 4-hydroxytamoxifen specifically in the intestinal epithelial cells. The organoids will then be maintained in conditioned media for 7 days to enable Cas9-mediated editing of APC, and then maintained in media without WNT3A or R-spondin-1 supplemented with N2 and B27 to select for APC-deficient organoids. This results in development of single tumors. Orthotopic transplantation of the transformed organoids will then be performed by mechanically removing the organoids, resuspending them in 90% minimal media and 10% Matrigel, and then transplanting them into recipient mice. Colonoscopy will then be performed 6 weeks later to assess tumor formation [78].

In-situ gene editing and orthotopic organoid transplantation is an advantageous way to model CRC compared to other CRC models: capture of the whole range of tumor progression; accuracy

of inducing the tumors in the appropriate tissue compartment and tissue layer; the requirement of only one gene loss - APC - for orthotopic engraftment rather than multiple mutations; fast formation of tumors within weeks; reproduce characteristic pathological features of human CRC; fast induction of tumors with defined CRISPR-Cas9-based gene alterations rather than the slow generation of germline mutations [78].

### Experimental Validation of MEK, mTOR, and PI3K Pathway Inhibition by AZD6244.2014 and AZD6244.8186 in AK CRC

Western Blot analysis of the phosphorylated proteins immediately downstream of the drug-targeted proteins will be performed to validate how effectively AZD6244.2014 and AZD6244.8186 inhibit their target pathways. For AZD6244.2014, the targets are MEK and mTOR, and therefore the phosphorylated proteins to be analyzed in Western blot would be phospho-ERK and phospho-rps6. For AZD6244.8186, the targets are MEK and PI3KB, and therefore the phosphorylated proteins to be analyzed in Western blot would be phospho-ERK and phospho-AKT. The cell/tumor samples will be of three groups: AZD6244.2014-treated, AZD6244.8186-treated, and drug vehicle-treated. The drug vehicle-treated cell/tumor sample will be used to control for combination therapy-treated cell/tumor samples, and β-actin will be used as loading control.

**Western Blot**: the AK CRC cell/tumor samples will be washed, lysed in RIPA lysis buffer, and centrifuged for 30 minutes at 4°C. The lysate will be extracted and a small volume will be taken for protein quantification assay to determine the protein concentration to be loaded into the gel. To the determined amount of protein, an equal volume of laemmli sample buffer will be added. The protein samples will be loaded into individual wells of the SDS-PAGE gel as well as the molecular weight marker and the loading control β-actin. The gel will be run in a running buffer for 1 hour at 100V and then the separated proteins will be transferred to a nitrocellulose membrane through a transfer buffer. To check the successful transfer of the proteins to the membrane, the membrane will be stained with Ponceau S. Then, the membrane will be blocked for 1 hour at room temperature using 3–5% milk. The membrane will then be incubated with properly diluted primary antibodies (phospho-ERK, phospho-rps6, phospho-AKT, β-actin) in blocking buffer overnight at

4°C. The membrane is washed with tris-buffered saline and Tween 20 (TBST) and incubated with secondary antibody (goat anti-mouse IgG) in blocking buffer at room temperature for 1 hour. The membrane is washed again with TBST and a chemiluminescence reaction will be developed to acquire an image of the Western blotting results [79].

Western blots is an effective early diagnostic tool that can detect picogram levels of protein in a sample. It is highly specific as it separates sample proteins based on size which can then be compared to standards of known molecular weights. Western blot is also highly selective due to the selective nature of the antibody-antigen interaction. However, there are limitations to Western blot: the formation of air bubbles during protein transfer that may skew band reading; potential non-specific binding of antibodies; potential high background and signal variability [80]. Alternatively, enzyme-linked immunosorbent assay (ELISA) can be used to quantify the phospho-target protein levels and offers distinct improvements such as being in 96-well plate format, less time consuming, and more sensitive [81].

### Experimental Validation of Metabolic Modulation by AZD6244.2014 and AZD6244.8186 in AK CRC

Small interfering RNA (siRNA) transfection targeting NRF2 and an ROS assay will be performed to validate the modulation of metabolic processes by AZD6244.2014 and AZD6244.8186 treatment in AK CRC. NRF2 is considered a master regulator of metabolism through its role as a redox-sensitive transcription factor controlling the expression of detoxification enzymes that protect the cells against oxidative stress [82, 83]. When silenced, NRF2 can no longer support cellular response to ROS stress, and the cells becomes more oxidative [82]. The cell/tumor samples will be of three groups: AZD6244.2014-treated, AZD6244.8186-treated, and drug vehicle-treated. The drug vehicle-treated cell/tumor sample will be used to control for combination therapy-treated cell/tumor samples, NRF2-targeting siRNA as positive control, and non-targeting siRNA as negative control.

**NRF2 siRNA transfection**: the AK CRC cell/tumor samples will first be washed with ice-cold PBS. After aspirating the PBS, the cells will be spun down and resuspended with Accell siRNA Delivery Media (Dharmacon). Dilution of 1x NRF2 siRNA Buffer is prepared by mixing four parts

sterile RNase-free water with one part 5x NRF2 siRNA Buffer (Dharmacon). 100μM NRF2 siRNA solution in 1x NRF2 siRNA buffer is then prepared and mixed for 90 minutes at 37°C. In each well of the well plate, 7.5μL of the 100 μM NRF2 siRNA solution and 750μL of the cells + Delivery Media mix are added, mixed, and incubated at 37°C with 5% CO2 for 72 hours [83, 84]. An antioxidant rescue effect will then be performed by adding N-acetyl cystine.

**ROS assay**: the NRF2 siRNA transfected AK CRC cell/tumor samples will be placed in a 96 well plate to which carboxy-$H_2$DCFDA will be added and mixed. The plate will be incubated for 3 hours at 37°C. The fluorescence of oxidized carboxy-$H_2$DCF will be measured by a FAC Scan flow cytometer at 488 nm excitation wavelength and 525 nm emission wavelength [82, 85].

### Experimental Validation of Immune Modulation by AZD6244.2014 and AZD6244.8186 in AK CRC

A cytokine array experiment will be performed to identify cytokines which were regulated in response to AZD6244.2014 and AZD6244.8186 treatment in AKA CRC. This will be followed by the incubation of commercial recombinant cytokines in a tumor conditioned immune cell culture to observe changes in phenotype or activation of the immune cells that confirm the immune-modulatory impact of the combination treatments. The cell/tumor samples will be of three groups: AZD6244.2014-treated, AZD6244.8186-treated, and drug vehicle-treated. The drug vehicle-treated cell/tumor sample will be used to control for combination therapy-treated cell/tumor samples.

**Cytokine Array**: an 8-well tray with an array membrane will be blocked by incubation with blocking buffer for 30 minutes. After aspirating the blocking buffer from each well, the appropriately diluted AK CRC cell/tumor lysate samples will be pipetted into each well and incubated for 2 hours. The samples will then be aspirated, wells washed, and biotin-conjugated anti-cytokines will be pipetted into each well and incubate for 2 hours. The wells aspirated and washed, HRP-conjugated streptavidin will be pipetted into each well and incubate for 2 hours. The wells aspirated and the membrane washed, the membrane will be transferred onto a sheet of chromatography paper and transferred onto a plastic sheet, to which a 1:1 mixture of detection

buffer will then be pipetted and incubated for 2 minutes. Another plastic sheet will be placed on top so the membrane is sandwiched between two plastic sheets, and the sandwiched membranes will then be transferred for chemiluminescence detection [86].

Cytokine arrays are advantageous to common ELISA cytokine detection as the arrays offer greater sensitivity, increased range of detection, and better precision. Furthermore, arrays' holistic view of cytokine expression compared to ELISA's single-target provides more data with less sample [86].

**Immune cell conditioned media**: the AK CRC cell/tumor samples will be incubated in 0.2% FBS medium + antibiotic-antimycotic agents (penicillin, streptomycin, amphotericin B) for 48 hours. The resulting conditioned media will be harvested, centrifuged for 10 minutes to remove suspended cells, and passed through a 0.22μm filter. The supernatant will then be reconstituted with 10% FBS [87, 88].

### Experimental Validation of CRIS-B Associated TGFβ Activity Changes by AZD6244.2014 and AZD6244.8186 in AK CRC

A sandwich ELISA assay will be performed to quantify TGFβ levels to validate the decrease of TGFβ activity associated with the subtype shift away from CRIS-B by AZD6244.2014 and AZD6244.8186. The cell/tumor samples to be used for sandwich ELISA will be of three groups: AZD6244.2014-treated, AZD6244.8186-treated, and drug vehicle-treated. The drug vehicle-treated cell/tumor sample will be used to control for combination therapy-treated cell/tumor samples.

**Sandwich ELISA**: the AK CRC cell/tumor samples will first be spun down to a supernatant, diluted with Assay Buffer (ABCAM) and HCl, mixed and incubated for 1 hour at room temperature. The mix will then be neutralized by NaOH. A standard dilution of the mouse TGFβ1 Stock Standard (ABCAM) will then be prepared (**table 2**) for a standard curve using distilled water as a diluent. To a 96-well microplate washed with wash buffer, The prepared standard dilutions will be added to their assigned wells, and the AK CRC cell/tumor lysates + Assay Buffer will be added to

the sample wells  in duplicate. After film-covered incubation at room temperature for 2 hours on a shaker, the wells will be emptied and washed. Biotin-Conjugated Antibody (ABCAM) will be added to all wells. After another round of film-covered incubation at room temperature for 1 hour on a shaker, the wells will be emptied and washed. Streptavidin-HRP (ABCAM) will be added to all wells. After another round of film-covered incubation at room temperature for 30 minutes on a shaker, the wells will be emptied and washed. TMB Substrate Solution (ABCAM) is added to all wells. After a final round of incubation at room temperature for 30 minutes, a stop solution will be added into each well when standard 1 has reached an OD of 0.9 - 0.95 at 620 nm as monitored by an ELISA reader. Absorbance of the samples and standards on each microplate is then read on a spectrophotometer using 620 nm as the reference wave length [89].

Sandwich ELISA is marked by high specificity as it utilizes two antibodies detecting different epitopes on the same antigen and high flexibility as it can accommodate both direct and indirect ELISA methods and can be used for complex samples. However, only monoclonal antibodies can be used as matched pairs because only monoclonals recognize specific antigen epitopes, making the experiment costly and too specific. Sandwich ELISA also requires a demanding design of finding two antibodies against the same target that recognize different epitopes and work well together can be challenging at times [90, 91].

**Table 2. Standard Dilutions for TGFβ Sandwich ELISA**

| Standard # | Sample to Dilute | Volume of Diluent (µL) | Starting Concentration (pg/ml) | Finishing Concentration (pg/ml) |
|---|---|---|---|---|
| 1 | Stock standard | 225 | 4000 | 2000 |
| 2 | Standard 1 | 225 | 2000 | 1000 |
| 3 | Standard 2 | 225 | 1000 | 500 |
| 4 | Standard 3 | 225 | 500 | 250 |
| 5 | Standard 4 | 225 | 250 | 125 |
| 6 | Standard 5 | 225 | 125 | 62.5 |
| 7 | Standard 6 | 225 | 62.5 | 31.3 |
| Blank | None | 225 | None | 0 |

## Therapeutics and Clinical Trials

The MEK, mTOR, and PI3K pathways are not only commonly dysregulated in CRC but in many different cancers as well, and hence these signaling cascades are targets to a wide range of approved and investigational inhibitors. MEK can be targeted by AZD6244 (selumetinib), trametinib, cobimetinib, and binimetinib, all of which are FDA approved MEK inhibitors currently investigated for the treatment of numerous cancers including CRC [92-95]. mTOR can also targeted by a wide range of available inhibitors including the second generation mTOR inhibitor AZD2014 (vistusertib) and the approved first generation mTOR inhibitors sirolimus, temsirolimus, and everolimus [96-99]. AZD2014 is particularly promising for its dual inhibition of mTOR1and mTOR2, leading to a more effective cancer growth suppression [96]. Additionally, the PI3K pathway is the target of the investigational PI3KB inhibitor AZD8186 and the approved PI3KD inhibitors idelalisib, copanlisib, and duvelisib [100-103].

The efficacy of these inhibitors can be further optimized in combination with other therapeutic agents to drive improved therapeutics in CRC. For example, the targeted pathway inhibitors can be potentially beneficial with the anti-neoplastic enzyme inhibitor irinotecan, which is approved for the treatment of metastatic CRC, in KRAS mutated CRC [104]. In EGFR-sensitive wild type KRAS CRC, the efficacy of the pathway inhibitors can be amplified by co-administering EGFR inhibitors such as cetuximab [105]. Furthermore, the targeted pathway inhibitors may potentially be combined with chemotherapeutic agents such as 5-fluorouracil or capecitabine in advanced tumor stages to slow cancer progression during systemic therapy [106]. Different targeted pathway inhibitors may also be used in combination with each other as demonstrated in this report and as studied in multiple current clinical trials [107-111]. Previously established as the rationale for using combination targeted pathway inhibitors rather than monotherapies in this research project, inhibiting multiple pathways downstream of RAS simultaneously can block cancer resistance mechanisms of activating parallel pathways to maintain proliferation and hence optimize therapeutic efficacy [16, 17, 19].

There is a multitude of clinical trials investigating targeted pathway inhibitors in combination with other treatments **(table 3**). While active clinical trials investigating combination treatments

AZD6244.2014 and AZD6244.8186 are primarily in breast and lung cancers [107, 108] but none in CRC, this highlights the novelty of using AZD6244.2014 and AZD6244.8186 in human CRC populations to offer the improved prognosis and survival demonstrated in the results of this project. AZD6244.2014 is being investigated in a phase Ib/IIa clinical study NCT02583542 against triple-negative breast cancer, squamous cell lung cancer and non-squamous cell lung cancer with wild type or mutated KRAS [107], and AZD6244.8186 is being investigated in a phase I study NCT01884285 against triple negative breast cancer, squamous non-small cell lung cancer, and castrate-resistant prostate cancer [108]. Furthermore, MEK inhibitor trametinib is being evaluated in combination with immunotherapies such as nivolumab, ipilimumab, and durvalumab in multiple CRC clinical trials: NCT03377361 studies trametinib + nivolumab with or without Ipilimumab in pre-treated metastatic CRC [112] and NCT03428126 studies trametinib + immune checkpoint inhibitor durvalumab in microsatellite stable CRC [113]. Additionally, mTOR inhibitor everolimus is being evaluated with VEGF inhibitor bevacizumab for the treatment of for metastatic CRC in the phase II study NCT00597506 [114]. The overall diversity of treatments being investigated with the pathway inhibitors demonstrate the versatility of these targeted inhibitors in being used in combination with a wide range of therapeutic approaches.

The targeted pathways can be employed as predictive biomarkers in clinical trials. Since MEK, mTOR, and PI3K inhibitors exert their therapeutic effect by suppressing the phosphorylation of these signaling molecules and thereby suppressing the phosphorylation of their downstream cascades, predictive biomarkers for inhibitors would be phosphorylated proteins immediately downstream of the targeted signaling molecule. Predictive biomarkers for MEK, mTOR, and PI3K inhibitors would therefore be phospho-ERK, phospho-rps6, and phospho-AKT respectively.

**Table 3. Combination Therapies and Clinical Trials**

| Combination Treatment | | Cancer | Clinical Trial NCT # |
|---|---|---|---|
| **AZD6244** (MEK inhibitor) | **irinotecan** (chemotherapy) | Colorectal Cancer | NCT01116271 |
| **AZD6244** (MEK inhibitor) | **cetuximab** (EGFR inhibitor) | Colorectal Cancer | NCT01287130 |
| **AZD6244** (MEK inhibitor) | **capecitabine** (chemotherapy) | Metastatic Colorectal Cancer | NCT00514761 |
| **AZD6244** (MEK inhibitor) | **AZD2014** (mTOR inhibitor) | Triple-Negative Breast Cancer<br>Squamous Cell Lung Cancer<br>Non-Squamous Cell Lung Cancer | NCT02583542 |
| **AZD6244** (MEK inhibitor) | **AZD8186** (PI3KB inhibitor) | Triple-Negative Breast Cancer<br>Squamous Non-Small Cell Lung Cancer<br>Castrate-Resistant Prostate Cancer | NCT01884285 |
| **trametinib** (MEK inhibitor) | **nivolumab** (PD1 inhibitor)<br>**ipilimumab** (CTLA4 inhibitor) | Metastatic Colorectal Cancer | NCT03377361 |
| **trametinib** (MEK inhibitor) | **durvalumab** (PDL1 inhibitor) | Metastatic Colorectal Cancer | NCT03428126 |
| **everolimus** (mTOR inhibitor) | **bevacizumab** (VEGF inhibitor) | Metastatic Colorectal Cancer | NCT00597506 |

## Discussion

This report accounts the identification of a combination therapeutic approach which effectively suppresses its target pathways and impacts the metabolic and immune related cellular processes of AK CRC cells in vivo. Also more importantly, an unbiased analysis of the transcriptional profiles of the AK CRC cells in the presence and absence of the treatment revealed that the combination therapies shift the CRC subtype from an aggressive poor prognostic signature to a better prognostic signatures with extended DFS.

The most defining characteristic of cancer cells is their capacity to sustain proliferative signaling, which is a fundamental hallmark of cancer [115]. It is through sustained proliferation that cancer cells not only support their growth and survival but also influence other cellular functions [115]. One key impacted cellular function is metabolism, which cancer cells hijack its physiological processes to reprogram them into oncogenic metabolic pathways such as the Warburg aerobic glycolysis

and the consequent induction of ROS-mediated hypoxia [115-117]. This reprogramming of normal cell metabolism into cancer promoting processes have emerged as defining hallmarks of cancer in 2011, and has become the subject to intensive research since. On the genetic level, the oncogenic metabolic processes are associated with dysregulated RAS activation [115], which overstimulates its downstream pathways such as MEK, mTOR, and PI3K to express these oncogenic metabolic processes [10, 12-19, 116]. Hence, in a KRAS mutated CRC, a combination therapeutic approach that inhibits these parallel pathways simultaneously can suppress cancer cell proliferation and consequently impact the associated oncogenic metabolic processes, which is precisely what has been demonstrated by AZD6244.2014 and AZD6244.8186 in this report.

In addition to impacting cellular functions such as metabolism, the hallmark of sustained cancer cell proliferation remains enabled and unchecked in tumors due to another hallmark of cancer associated with the immune system [115]. A repertoire of immune cell types play important roles in not only driving tumor-promoting inflammation but also in angiogenesis and consequent metastasis [115, 118, 119]. While the infiltration of immune cells into tumors may signify an attempt of cancer eradication by the immune system, there is another paradoxical side in which immune cells - particularly those associated with innate immune responses such as macrophages, neutrophils, mast cells, and myeloid progenitors - induce tumor-promoting inflammations that enables neoplastic progression [115, 120]. Furthermore, immune cells can also activate angiogenic factors such as CXC-chemokines and cytokines to facilitate invasion and metastasis [115, 121, 122]. The pro-angiogenic role of multiple immune CXC-chemokine signaling axises has been shown in a number of studies, some even demonstrating the potential role of CXC-chemokines as prognostic biomarkers [60-62, 123]. Such oncogenic immune processes are stimulated by dysregulated RAS activation [115] and its downstream signaling pathways [10, 12-19], and hence the combination therapeutic approach by AZD6244.2014 and AZD6244.8186 that concomitantly suppresses these parallel pathways can downregulate these associated oncogenic immune processes, which is what has been demonstrated in this report. Importantly, the downregulation of immune signature gene sets by the combination treatments does not mean that the cancers were shifted towards an immune phenotype but were rather driven by a suppression of cellular secretion of immune associated chemokines and cytokines.

Ultimately, the combination targeted therapeutic approach by AZD6244.2014 and AZD6244.8186 promises better prognosis and extended survival of aggressive human-like subtypes of CRC by impacting two hallmarks of cancer. This valuable therapeutic finding for an aggressive disease with rising incidence and dismal survival highlights the clinical significance of taking this model for further investigation in human organoids and eventually in clinical trials to further evaluate the potential therapeutic benefits established in this report for human populations.

## Acknowledgements

I would like to thank my supervisor Andrew Campbell for his insightful supervision and guidance in making this project a valuable learning experience, and express my gratitude to David McGuinness and John Cole for their invaluable support in understanding bioinformatics and using Galaxy softwares. I would also like to thank Kathryn Gilroy for her kind assistance in writing the R code for CRIS and CMS subtyping.

## References


1. Keum N, Giovannucci E. Global burden of colorectal cancer: emerging trends, risk factors and prevention strategies. Nature Reviews Gastroenterology & Hepatology. 2019;16(12):713-732.
2. Dienstmann R, Vermeulen L, Guinney J, Kopetz S, Tejpar S, Tabernero J. Consensus molecular subtypes and the evolution of precision medicine in colorectal cancer. Nature Reviews Cancer. 2017;17(2):79-92.
3. Xie Y, Chen Y, Fang J. Comprehensive review of targeted therapy for colorectal cancer. Signal Transduction and Targeted Therapy. 2020;5(1).
4. Kuipers E, Grady W, Lieberman D, Seufferlein T, Sung J, Boelens P et al. Colorectal cancer. Nature Reviews Disease Primers. 2015;1(1).
5. Rimbert J, Tachon G, Junca A, Villalva C, Karayan-Tapon L, Tougeron D. Association between clinicopathological characteristics and RAS mutation in colorectal cancer. Modern Pathology. 2017;31(3):517-526.
6. He Z, Thorrez L, Siegfried G, Meulemans S, Evrard S, Tejpar S et al. The proprotein convertase furin is a pro-oncogenic driver in KRAS and BRAF driven colorectal cancer. Oncogene. 2020;39(17):3571-3587.
7. Schell M, Yang M, Teer J, Lo F, Madan A, Coppola D et al. A multigene mutation classification of 468 colorectal cancers reveals a prognostic role for APC. Nature Communications. 2016;7(1).
8. Fearon E. Molecular Genetics of Colorectal Cancer. Annual Review of Pathology: Mechanisms of Disease. 2011;6(1):479-507.
9. Moore A, Rosenberg S, McCormick F, Malek S. RAS-targeted therapies: is the undruggable drugged?. Nature Reviews Drug Discovery. 2020;19(8):533-552.
10. Fang J, Richardson B. The MAPK signalling pathways and colorectal cancer. The Lancet Oncology. 2005;6(5):322-327.
11. Williams D, Mouradov D, Browne C, Palmieri M, Elliott M, Nightingale R et al. Overexpression of TP53 protein is associated with the lack of adjuvant chemotherapy benefit in patients with stage III colorectal cancer. Modern Pathology. 2019;33(3):483-495..

12. Denton C, Gustafson D. Pharmacokinetics and pharmacodynamics of AZD6244 (ARRY-142886) in tumor-bearing nude mice. Cancer Chemotherapy and Pharmacology. 2010;67(2):349-360.
13. Bhalla S, Evens A, Dai B, Prachand S, Gordon L, Gartenhaus R. The novel anti-MEK small molecule AZD6244 induces BIM-dependent and AKT-independent apoptosis in diffuse large B-cell lymphoma. Blood. 2011;118(4):1052-1061.
14. Lynch J, Polanska U, Delpuech O, Hancox U, Trinidad A, Michopoulos F et al. Inhibiting PI3Kβ with AZD8186 Regulates Key Metabolic Pathways in PTEN-Null Tumors. Clinical Cancer Research. 2017;23(24):7584-7595.
15. Hancox U, Cosulich S, Hanson L, Trigwell C, Lenaghan C, Ellston R et al. Inhibition of PI3K Signaling with AZD8186 Inhibits Growth of PTEN-Deficient Breast and Prostate Tumors Alone and in Combination with Docetaxel. Molecular Cancer Therapeutics. 2014;14(1):48-58.
16. Wang X, Ding J, Meng L. PI3K isoform-selective inhibitors: next-generation targeted cancer therapies. Acta Pharmacologica Sinica. 2015;36(10):1170-1176.
17. Francipane M, Lagasse E. mTOR pathway in colorectal cancer: an update. Oncotarget. 2013;5(1):49-66.
18. Guichard S, Curwen J, Bihani T, D'Cruz C, Yates J, Grondine M et al. AZD2014, an Inhibitor of mTORC1 and mTORC2, Is Highly Effective in ER+ Breast Cancer When Administered Using Intermittent or Continuous Schedules. Molecular Cancer Therapeutics. 2015;14(11): 2508-2518.
19. Wang X. Targeting mTOR network in colorectal cancer therapy. World Journal of Gastroenterology. 2014;20(15):4178.
20. Isella C, Brundu F, Bellomo S, Galimi F, Zanella E, Porporato R et al. Selective analysis of cancer-cell intrinsic transcriptional traits defines novel clinically relevant subtypes of colorectal cancer. Nature Communications. 2017;8(1).
21. Dienstmann R, Guinney J, Delorenzi M, De Reynies A, Roepman P, Sadanandam A et al. Colorectal Cancer Subtyping Consortium (CRCSC) identification of a consensus of molecular subtypes. Journal of Clinical Oncology. 2014;32(15_suppl):3511-3511.
22. Simoneaux R. The Four Colorectal Cancer Consensus Molecular Subtypes. Oncology Times. 2018;40(6):10-11.

23. Eide P, Bruun J, Lothe R, Sveen A. CMScaller: an R package for consensus molecular subtyping of colorectal cancer pre-clinical models. Scientific Reports. 2017;7(1).
24. Jackstadt R, van Hooff S, Leach J, Cortes-Lavaud X, Lohuis J, Ridgway R et al. Epithelial NOTCH Signaling Rewires the Tumor Microenvironment of Colorectal Cancer to Drive Poor-Prognosis Subtypes and Metastasis. Cancer Cell. 2019;36(3):319-336.e7.
25. Dry J, Pavey S, Pratilas C, Harbron C, Runswick S, Hodgson D et al. Transcriptional Pathway Signatures Predict MEK Addiction and Response to Selumetinib (AZD6244). Cancer Research. 2010;70(6):2264-2273.
26. Ammar H, Closset J. Clusterin Activates Survival through the Phosphatidylinositol 3-Kinase/Akt Pathway. Journal of Biological Chemistry. 2008;283(19):12851-12861.
27. Xu L, Hu H, Zheng L, Wang M, Mei Y, Peng L et al. ETV4 is a theranostic target in clear cell renal cell carcinoma that promotes metastasis by activating the pro-metastatic gene FOSL1 in a PI3K-AKT dependent manner. Cancer Letters. 2020;482:74-89.
28. Aytes A, Mitrofanova A, Kinkade C, Lefebvre C, Lei M, Phelan V et al. ETV4 promotes metastasis in response to activation of PI3-kinase and Ras signaling in a mouse model of advanced prostate cancer. Proceedings of the National Academy of Sciences. 2013;110(37):E3506-E3515.
29. Meng D, Li Z, Ma X, Wu L, Fu L, Qin G. ETV5 overexpression contributes to tumor growth and progression of thyroid cancer through PIK3CA. Life Sciences. 2020;253:117693.
30. Li S, Ma Y, Zheng P, Zhang P. GDF15 promotes the proliferation of cervical cancer cells by phosphorylating AKT1 and Erk1/2 through the receptor ErbB2. Journal of Experimental & Clinical Cancer Research. 2018;37(1).
31. Li A, Gu Y, Li X, Sun H, Zha H, Xie J et al. S100A6 promotes the proliferation and migration of cervical cancer cells via the PI3K/Akt signaling pathway. Oncology Letters. 2018;;5685–93.
32. Li Z, Tang M, Ling B, Liu S, Zheng Y, Nie C et al. Increased expression of S100A6 promotes cell proliferation and migration in human hepatocellular carcinoma. Journal of Molecular Medicine. 2013;92(3):291-303.
33. Cole, J.J., Faydaci, B., Megalios, A., Shaw, R., Robertson, N., Goodyear, C.S. Searchlight 2: Rapid and comprehensive RNA-seq data exploration and visualisation for unlimited differential datasets. 2018-2019. https://github.com/Searchlight2/Searchlight2/

34. Katagiri M, Karasawa H, Takagi K, et al. Hexokinase 2 in colorectal cancer: a potent prognostic factor associated with glycolysis, proliferation and migration. Histol Histopathol. 2017;32(4):351-360.
35. Kudryavtseva A, Fedorova M, Zhavoronkov A, Moskalev A, Zasedatelev A, Dmitriev A et al. Effect of lentivirus-mediated shRNA inactivation of HK1, HK2, and HK3 genes in colorectal cancer and melanoma cells. BMC Genetics. 2016, 17(Suppl 3):156
36. Li W, Huang C, Hsieh Y, Chen T, Cheng L, Chen C et al. Regulatory Role of Hexokinase 2 in Modulating Head and Neck Tumorigenesis. Frontiers in Oncology. 2020;10:176.
37. Patra K, Wang Q, Bhaskar P, Miller L, Wang Z, Wheaton W et al. Hexokinase 2 Is Required for Tumor Initiation and Maintenance and Its Systemic Deletion Is Therapeutic in Mouse Models of Cancer. Cancer Cell. 2013;24(3):399.
38. Wu J, Hu L, Wu F, Zou L, He T. Poor prognosis of hexokinase 2 overexpression in solid tumors of digestive system: a meta-analysis. Oncotarget. 2017;8(19):32332-32344.
39. Kwon Y, Baek H, Ye D, Shin S, Chun Y. CYP1B1 enhances cell proliferation and metastasis through induction of EMT and activation of WNT/B-catenin signaling via Sp1 upregulation. Drug Metabolism and Pharmacokinetics. 2017;32(1):S38-S39.
40. Chang I, Mitsui Y, Kim S, Sun J, Jeon H, Kang J et al. Cytochrome P450 1B1 inhibition suppresses tumorigenicity of prostate cancer via caspase-1 activation. Oncotarget. 2017;8(24):39087-39100.
41. Morel F, Aninat C. The glutathione transferase kappa family. Drug Metabolism Reviews. 2011;43(2):281-291.
42. Economopoulos K, Sergentanis T. GSTM1, GSTT1, GSTP1, GSTA1 and colorectal cancer risk: A comprehensive meta-analysis. European Journal of Cancer. 2010;46(9):1617-1631.
43. Hashibe M, McKay J, Curado M, Oliveira J, Koifman S, Koifman R et al. Multiple ADH genes are associated with upper aerodigestive cancers. Nature Genetics. 2008;40(6):707-709.
44. Yang W, Wang Y, Wang W, Chen Z, Bai G. Expression of Aldehyde Dehydrogenase 1A1 (ALDH1A1) as a Prognostic Biomarker in Colorectal Cancer Using Immunohistochemistry. Medical Science Monitor. 2018;24:2864-2872.
45. Jette C, Peterson P, Sandoval I, Manos E, Hadley E, Ireland C et al. The Tumor Suppressor Adenomatous Polyposis Coli and Caudal Related Homeodomain Protein Regulate Expression of Retinol Dehydrogenase L. Journal of Biological Chemistry. 2004;279(33):34397-34405.

46. Cheng Y, Pincas H, Huang J, Zachariah E, Zeng Z, Notterman D et al. High incidence of LRAT promoter hypermethylation in colorectal cancer correlates with tumor stage. Medical Oncology. 2014;31(11).
47. MacFie T, Poulsom R, Parker A, Warnes G, Boitsova T, Nijhuis A et al. DUOX2 and DUOXA2 Form the Predominant Enzyme System Capable of Producing the Reactive Oxygen Species H2O2 in Active Ulcerative Colitis and are Modulated by 5-Aminosalicylic Acid. Inflammatory Bowel Diseases. 2014;20(3):514-524.
48. Rigoni A, Poulsom R, Jeffery R, Mehta S, Lewis A, Yau C et al. Separation of Dual Oxidase 2 and Lactoperoxidase Expression in Intestinal Crypts and Species Differences May Limit Hydrogen Peroxide Scavenging During Mucosal Healing in Mice and Humans. Inflammatory Bowel Diseases. 2017;24(1):136-148.
49. Xue X, Jungles K, Onder G, Samhoun J, Győrffy B, Hardiman K. HIF-3α1 promotes colorectal tumor cell growth by activation of JAK-STAT3 signaling. Oncotarget. 2016;7(10):11567-11579.
50. Ma X, Zhang H, Xue X, Shah Y. Hypoxia-inducible factor 2α (HIF-2α) promotes colon cancer growth by potentiating Yes-associated protein 1 (YAP1) activity. Journal of Biological Chemistry. 2017;292(41):17046-17056.
51. Thomas D, Wink D. NOS2 as an Emergent Player in Progression of Cancer. Antioxidants & Redox Signaling. 2017;26(17):963-965.
52. Heinecke J, Ridnour L, Cheng R, Switzer C, Lizardo M, Khanna C et al. Tumor microenvironment-based feed-forward regulation of NOS2 in breast cancer progression. Proceedings of the National Academy of Sciences. 2014;111(17):6323-6328.
53. Basudhar D, Somasundaram V, de Oliveira G, Kesarwala A, Heinecke J, Cheng R et al. Nitric Oxide Synthase-2-Derived Nitric Oxide Drives Multiple Pathways of Breast Cancer Progression. Antioxidants & Redox Signaling. 2017;26(18):1044-1058.
54. Yang Z, Bai Y, Huo L, Chen H, Huang J, Li J et al. Expression of A disintegrin and metalloprotease 8 is associated with cell growth and poor survival in colorectal cancer. BMC Cancer. 2014;14(1).
55. Dreymueller D, Pruessmeyer J, Schumacher J, Fellendorf S, Hess F, Seifert A et al. The metalloproteinase ADAM8 promotes leukocyte recruitment in vitro and in acute lung inflammation. American Journal of Physiology-Lung Cellular and Molecular Physiology. 2017;313(3):L602-L614.

56. Conrad C, Benzel J, Dorzweiler K, Cook L, Schlomann U, Zarbock A et al. ADAM8 in invasive cancers: links to tumor progression, metastasis, and chemoresistance. Clinical Science. 2019;133(1):83-99.
57. Hagihara T, Kondo J, Endo H, Ohue M, Sakai Y, Inoue M. Hydrodynamic stress stimulates growth of cell clusters via the ANXA1/PI3K/AKT axis in colorectal cancer. Scientific Reports. 2019;9(1).
58. Boudhraa Z, Bouchon B, Viallard C, D'Incan M, Degoul F. Annexin A1 localization and its relevance to cancer. Clinical Science. 2016;130(4):205-220.
59. Gastardelo T, Cunha B, Raposo L, Maniglia J, Cury P, Lisoni F et al. Inflammation and Cancer: Role of Annexin A1 and FPR2/ALX in Proliferation and Metastasis in Human Laryngeal Squamous Cell Carcinoma. PLoS ONE. 2014;9(12):e111317.
60. Lim S, Yuzhalin A, Gordon-Weeks A, Muschel R. Targeting the CCL2-CCR2 signaling axis in cancer metastasis. Oncotarget. 2016;7(19):28697-28710.
61. Zhu Z, Zhang X, Guo H, Fu L, Pan G, Sun Y. CXCL13-CXCR5 axis promotes the growth and invasion of colon cancer cells via PI3K/AKT pathway. Molecular and Cellular Biochemistry. 2014;400(1-2):287-295.
62. Frick VO, Rubie C, Keilholz U, Ghadjar P. Chemokine/chemokine receptor pair CCL20/CCR6 in human colorectal malignancy: An overview. World J Gastroenterol. 2016;22(2):833-841.
63. Greenow KR, Zverev M, May S, et al. Lect2 deficiency is characterised by altered cytokine levels and promotion of intestinal tumourigenesis. Oncotarget. 2018;9(92):36430-36443.
64. Perkins N. The diverse and complex roles of NF-κB subunits in cancer. Nature Reviews Cancer. 2012;12(2):121-132.
65. Myant K, Cammareri P, McGhee E, Ridgway R, Huels D, Cordero J et al. ROS Production and NF-κB Activation Triggered by RAC1 Facilitate WNT-Driven Intestinal Stem Cell Proliferation and Colorectal Cancer Initiation. 2013;12(6):761–73.
66. Pelicci P, Dalton P, Giorgio M. The Other Face of ROS: a Driver of Stem Cell Expansion in Colorectal Cancer. 2013;12(6):635–6.
67. Colomer C, Margalef P, Gonzalez J, Vert A, Bigas A, Espinosa L. IKKα is required in the intestinal epithelial cells for tumour stemness. British Journal of Cancer. 2018;118(6):839-846.

68. Porta C, Ippolito A, Consonni F, Carraro L, Celesti G, Correale C et al. Protumor Steering of Cancer Inflammation by p50 NF-κB Enhances Colorectal Cancer Progression. Cancer Immunology Research. 2018;6(5):578-593.
69. Kawaguchi M, Yamamoto K, Kanemaru A, Tanaka H, Umezawa K, Fukushima T et al. Inhibition of nuclear factor-κB signaling suppresses Spint1-deletion-induced tumor susceptibility in the ApcMin/+ model. Oncotarget. 2016;7(42):68614-68622.
70. Yang X, Panopoulos A, Nurieva R, Chang S, Wang D, Watowich S et al. STAT3 Regulates Cytokine-mediated Generation of Inflammatory Helper T Cells. Journal of Biological Chemistry. 2007;282(13):9358-9363.
71. Mcilwain DR, Grusdat M, Pozdeev VI, Beyer M, Bergthaler A, Dieter H, et al. T-cell STAT3 is required for the maintenance of humoral immunity to LCMV. 2015;418–27.
72. STAT6 signal transducer and activator of transcription 6 [Homo sapiens (human)] - Gene - NCBI [Internet]. Ncbi.nlm.nih.gov. 2020 [cited 26 August 2020]. Available from: https://www.ncbi.nlm.nih.gov/gene/6778
73. POU2F2 POU class 2 homeobox 2 [Homo sapiens (human)] - Gene - NCBI [Internet]. Ncbi.nlm.nih.gov. 2020 [cited 26 August 2020]. Available from: https://www.ncbi.nlm.nih.gov/gene/5452
74. Wang S, Tie J, Wang W, Hu S, Yin J, Yi X et al. POU2F2-oriented network promotes human gastric cancer metastasis. Gut. 2015;65(9):1427-1438.
75. NR1I3 - nuclear receptor subfamily 1 group I member 3 (human) [Internet]. Pubchem.ncbi.nlm.nih.gov. 2020 [cited 26 August 2020]. Available from: https://pubchem.ncbi.nlm.nih.gov/gene/NR1I3/human
76. Vlahopoulos S, Logotheti S, Mikas D, Giarika A, Gorgoulis V, Zoumpourlis V. The role of ATF-2 in oncogenesis. BioEssays. 2008;30(4):314-327.
77. Olofsson L, Orho-Melander M, William-Olsson L, Sjöholm K, Sjöström L, Groop L et al. CCAAT/Enhancer Binding Protein α (C/EBPα) in Adipose Tissue Regulates Genes in Lipid and Glucose Metabolism and a Genetic Variation in C/EBPα Is Associated with Serum Levels of Triglycerides. The Journal of Clinical Endocrinology & Metabolism. 2008;93(12):4880-4886.
78. Roper J, Tammela T, Cetinbas N, Akkad A, Roghanian A, Rickelt S et al. In vivo genome editing and organoid transplantation models of colorectal cancer and metastasis. Nature Biotechnology. 2017;35(6):569-576.

79. Western blot protocol | Abcam [Internet]. Abcam.com. 2020 [cited 26 August 2020]. Available from: https://www.abcam.com/protocols/general-western-blot-protocol
80. Ghosh R, Gilda JE, Gomes AV. The necessity of and strategies for improving confidence in the accuracy of western blots. Expert Rev Proteomics. 2014;11(5):549-560.
81. Bass J, Wilkinson D, Rankin D, Phillips B, Szewczyk N, Smith K et al. An overview of technical considerations for Western blotting applications to physiological research. Scandinavian Journal of Medicine & Science in Sports. 2016;27(1):4-25.
82. Singh A, Boldin-Adamsky S, Thimmulappa R, Rath S, Ashush H, Coulter J et al. RNAi-Mediated Silencing of Nuclear Factor Erythroid-2-Related Factor 2 Gene Expression in Non-Small Cell Lung Cancer Inhibits Tumor Growth and Increases Efficacy of Chemotherapy. Cancer Research. 2008;68(19):7975-7984.
83. Bozaykut P, Ozer N, Karademir B. Nrf2 silencing to inhibit proteolytic defense induced by hyperthermia in HT22 cells. Redox Biology. 2016;8:323-332.
84. Accell siRNA Reagents - Rat [Internet]. Horizondiscovery.com. 2020 [cited 26 August 2020]. Available from: https://horizondiscovery.com/en/products/gene-modulation/knockdown-reagents/sirna/PIFs/Accell-siRNA-Reagents-Rat#specifications
85. Schafer Z, Grassian A, Song L, Jiang Z, Gerhart-Hines Z, Irie H et al. Antioxidant and oncogene rescue of metabolic defects caused by loss of matrix attachment. Nature. 2009;461(7260):109-113.
86. Cytokine Array – Mouse Cytokine Antibody Array (Membrane, 22 Targets) (ab133993) [Internet]. Abcam.com. 2020 [cited 26 August 2020]. Available from: https://www.abcam.com/cytokine-array-mouse-cytokine-antibody-array-membrane-22-targets-ab133993.html
87. Cohen E, Gao H, Anfossi S, Mego M, Reddy N, Debeb B et al. Inflammation Mediated Metastasis: Immune Induced Epithelial-To-Mesenchymal Transition in Inflammatory Breast Cancer Cells. PLOS ONE. 2015;10(7):e0132710.
88. Benner B, Scarberry L, Suarez-Kelly L, Duggan M, Campbell A, Smith E et al. Generation of monocyte-derived tumor-associated macrophages using tumor-conditioned media provides a novel method to study tumor-associated macrophages in vitro. Journal for ImmunoTherapy of Cancer. 2019;7(1).

89. (ab119558) R. Rat TGF beta 1 ELISA Kit (ab119558) | Abcam [Internet]. Abcam.com. 2020 [cited 26 August 2020]. Available from: https://www.abcam.com/rat-tgf-beta-1-elisa-kit-ab119558.html
90. ELISA Illustrated Assay [Internet]. Novus Biologicals. 2020 [cited 26 August 2020]. Available from: https://bourls.com/Rl0nR
91. Types of ELISA | Abcam [Internet]. Abcam.com. 2020 [cited 26 August 2020]. Available from: https://www.abcam.com/kits/types-of-elisa
92. Selumetinib - DrugBank [Internet]. Drugbank.ca. 2020 [cited 26 August 2020]. Available from: https://www.drugbank.ca/drugs/DB11689
93. Trametinib - DrugBank [Internet]. Drugbank.ca. 2020 [cited 26 August 2020]. Available from: https://www.drugbank.ca/drugs/DB08911
94. Cobimetinib - DrugBank [Internet]. Drugbank.ca. 2020 [cited 26 August 2020]. Available from: https://www.drugbank.ca/drugs/DB05239
95. Binimetinib - DrugBank [Internet]. Drugbank.ca. 2020 [cited 26 August 2020]. Available from: https://www.drugbank.ca/drugs/DB11967
96. AZD2014 | mTOR serine/threonine kinase inhibitor | TORC1 | TORC2 [Internet]. Openinnovation.astrazeneca.com. 2020 [cited 26 August 2020]. Available from: https://openinnovation.astrazeneca.com/azd2014.html
97. Sirolimus - DrugBank [Internet]. Drugbank.ca. 2020 [cited 26 August 2020]. Available from: https://www.drugbank.ca/drugs/DB00877
98. Temsirolimus - DrugBank [Internet]. Drugbank.ca. 2020 [cited 26 August 2020]. Available from: https://www.drugbank.ca/drugs/DB06287
99. Everolimus - DrugBank [Internet]. Drugbank.ca. 2020 [cited 26 August 2020]. Available from: https://www.drugbank.ca/drugs/DB01590
100. AZD8186 | PI3K beta & delta | Oncology | AstraZeneca Open Innovation [Internet]. Openinnovation.astrazeneca.com. 2020 [cited 26 August 2020]. Available from: https://openinnovation.astrazeneca.com/azd8186.html
101. Idelalisib - DrugBank [Internet]. Drugbank.ca. 2020 [cited 26 August 2020]. Available from: https://www.drugbank.ca/drugs/DB09054
102. Copanlisib - DrugBank [Internet]. Drugbank.ca. 2020 [cited 26 August 2020]. Available from: https://www.drugbank.ca/drugs/DB12483

103. Duvelisib - DrugBank [Internet]. Drugbank.ca. 2020 [cited 26 August 2020]. Available from: https://www.drugbank.ca/drugs/DB11952

104. Study of Selumetinib (AZD6244)(ARRY-142886) in Combination With Irinotecan in Previously Treated Patients With Colorec - Full Text View - ClinicalTrials.gov [Internet]. Bourls.com. 2020 [cited 26 August 2020]. Available from: https://bourls.com/CkvgX

105. AZD6244 With Cetuximab for Solid Tumors and Colorectal Cancer - Full Text View - ClinicalTrials.gov [Internet]. Bourls.com. 2020 [cited 26 August 2020]. Available from: https://bourls.com/tsS2l

106. Phase II Efficacy Study of AZD6244 in Colorectal Cancer - Full Text View - ClinicalTrials.gov [Internet]. Bourls.com. 2020 [cited 26 August 2020]. Available from: https://bourls.com/PGY1u

107. A Study of AZD2014 in Combination With Selumetinib in Patients With Advanced Cancers - Full Text View - ClinicalTrials.gov [Internet]. Bourls.com. 2020 [cited 26 August 2020]. Available from: https://bourls.com/hbKge

108. AZD8186 First Time In Patient Ascending Dose Study - Full Text View - ClinicalTrials.gov [Internet]. Bourls.com. 2020 [cited 26 August 2020]. Available from: https://bourls.com/aW5hs

109. TraMel-WT: A Trial of Trametinib in Patients With Advanced Pretreated BRAFV600 Wild-type Melanoma - Full Text View - ClinicalTrials.gov [Internet]. Bourls.com. 2020 [cited 26 August 2020]. Available from: https://bourls.com/HEsXt

110. Trametinib and Akt Inhibitor GSK2141795 in Treating Patients With Metastatic Triple-Negative Breast Cancer - Full Text View - ClinicalTrials.gov [Internet]. Bourls.com. 2020 [cited 26 August 2020]. Available from: https://bourls.com/13df4

111.Trametinib and Everolimus for the Treatment of Pediatric and Young Adult Patients With Recurrent Low Grade Gliomas (PNOC021) - Full Text View - ClinicalTrials.gov [Internet]. Bourls.com. 2020 [cited 26 August 2020]. Available from: https://bourls.com/dqZ6y

112. An Investigational Immuno-therapy Study Of Nivolumab In Combination With Trametinib With Or Without Ipilimumab In Patients With Previously Treated Cancer of the Colon or Rectum That Has Spread - Full Text View - ClinicalTrials.gov [Internet]. Bourls.com. 2020 [cited 26 August 2020]. Available from: https://bourls.com/HOppX

113. Study of Durvalumab (MEDI4736) (Anti-PD-L1) and Trametinib (MEKi) in MSS Metastatic Colon Cancer - Full Text View - ClinicalTrials.gov [Internet]. Bourls.com. 2020 [cited 26 August 2020]. Available from: https://bourls.com/jo39e

114. Expanded Cohort for Metastatic Colorectal Cancer (MCRC) Using Bevacizumab + Everolimus - Full Text View - ClinicalTrials.gov [Internet]. Bourls.com. 2020 [cited 26 August 2020]. Available from: https://bourls.com/XPRB4

115.Hanahan D, Weinberg R. Hallmarks of Cancer: The Next Generation. Cell. 2011;144(5): 646-674.

116. DeBerardinis R, Lum J, Hatzivassiliou G, Thompson C. The Biology of Cancer: Metabolic Reprogramming Fuels Cell Growth and Proliferation. Cell Metabolism. 2008;7(1):11-20.

117. Warburg O, Dickens F. The metabolism of tumours. London: Constable; 1930.

118. Murdoch C, Muthana M, Coffelt S, Lewis C. The role of myeloid cells in the promotion of tumour angiogenesis. Nature Reviews Cancer. 2008;8(8):618-631.

119. Zumsteg A, Christofori G. Corrupt policemen: inflammatory cells promote tumor angiogenesis. Current Opinion in Oncology. 2009;21(1):60-70.

120. Grivennikov S, Greten F, Karin M. Immunity, Inflammation, and Cancer. Cell. 2010;140(6): 883-899.

121. Arenberg D, Polverini P, Kunkel S, Shanafelt A, Hesselgesser J, Horuk R et al. The role of CXC chemokines in the regulation of angiogenesis in non-small cell lung cancer. Journal of Leukocyte Biology. 1997;62(5):554-562.

122. Itatani Y, Kawada K, Inamoto S, Yamamoto T, Ogawa R, Taketo M et al. The Role of Chemokines in Promoting Colorectal Cancer Invasion/Metastasis. International Journal of Molecular Sciences. 2016;17(5):643.

123. Heras S, Martínez-Balibrea E. CXC family of chemokines as prognostic or predictive biomarkers and possible drug targets in colorectal cancer. World Journal of Gastroenterology. 2018;24(42):4738-4749.

# Appendix

**(A)**

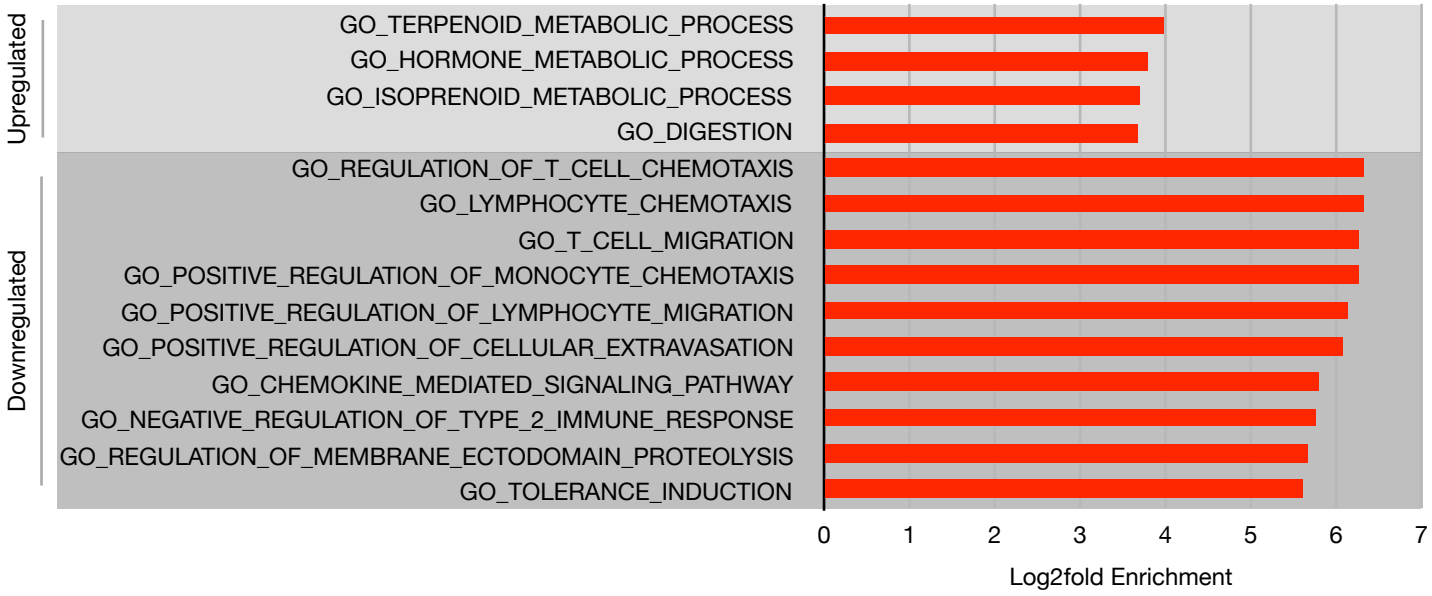
Upregulated
Downregulated
GO_TERPENOID_METABOLIC_PROCESS
GO_HORMONE_METABOLIC_PROCESS
GO_ISOPRENOID_METABOLIC_PROCESS
GO_DIGESTION
GO_REGULATION_OF_T_CELL_CHEMOTAXIS
GO_LYMPHOCYTE_CHEMOTAXIS
GO_T_CELL_MIGRATION
GO_POSITIVE_REGULATION_OF_MONOCYTE_CHEMOTAXIS
GO_POSITIVE_REGULATION_OF_LYMPHOCYTE_MIGRATION
GO_POSITIVE_REGULATION_OF_CELLULAR_EXTRAVASATION
GO_CHEMOKINE_MEDIATED_SIGNALING_PATHWAY
GO_NEGATIVE_REGULATION_OF_TYPE_2_IMMUNE_RESPONSE
GO_REGULATION_OF_MEMBRANE_ECTODOMAIN_PROTEOLYSIS
GO_TOLERANCE_INDUCTION
0
1
2
3
4
5
6
7
Log2fold Enrichment

**(B)**

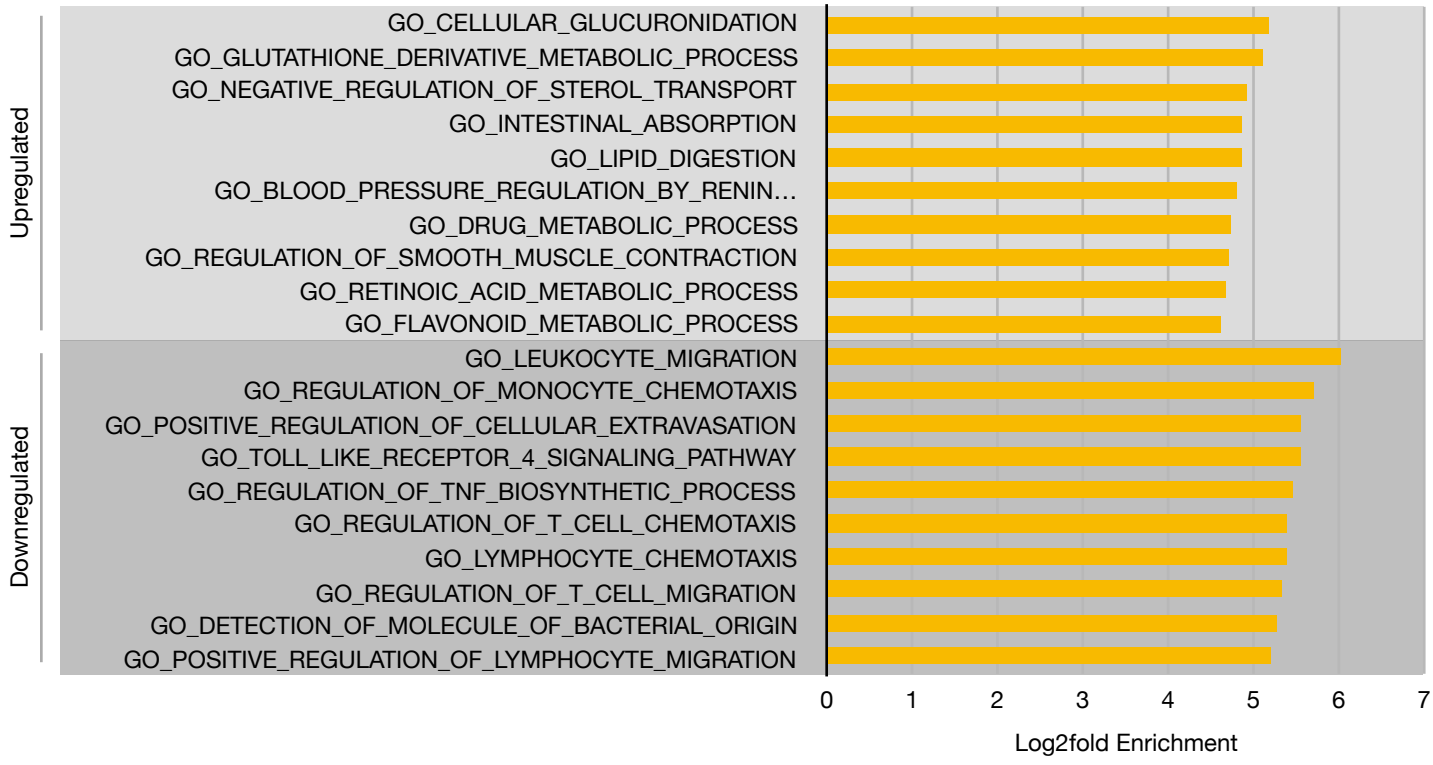
Upregulated
Downregulated
GO_CELLULAR_GLUCURONIDATION
GO_GLUTATHIONE_DERIVATIVE_METABOLIC_PROCESS
GO_NEGATIVE_REGULATION_OF_STEROL_TRANSPORT
GO_INTESTINAL_ABSORPTION
GO_LIPID_DIGESTION
GO_BLOOD_PRESSURE_REGULATION_BY_RENIN...
GO_DRUG_METABOLIC_PROCESS
GO_REGULATION_OF_SMOOTH_MUSCLE_CONTRACTION
GO_RETINOIC_ACID_METABOLIC_PROCESS
GO_FLAVONOID_METABOLIC_PROCESS
GO_LEUKOCYTE_MIGRATION
GO_REGULATION_OF_MONOCYTE_CHEMOTAXIS
GO_POSITIVE_REGULATION_OF_CELLULAR_EXTRAVASATION
GO_TOLL_LIKE_RECEPTOR_4_SIGNALING_PATHWAY
GO_REGULATION_OF_TNF_BIOSYNTHETIC_PROCESS
GO_REGULATION_OF_T_CELL_CHEMOTAXIS
GO_LYMPHOCYTE_CHEMOTAXIS
GO_REGULATION_OF_T_CELL_MIGRATION
GO_DETECTION_OF_MOLECULE_OF_BACTERIAL_ORIGIN
GO_POSITIVE_REGULATION_OF_LYMPHOCYTE_MIGRATION
0
1
2
3
4
5
6
7
Log2fold Enrichment
AZD6244.2014
AZD6244.8186

(C)

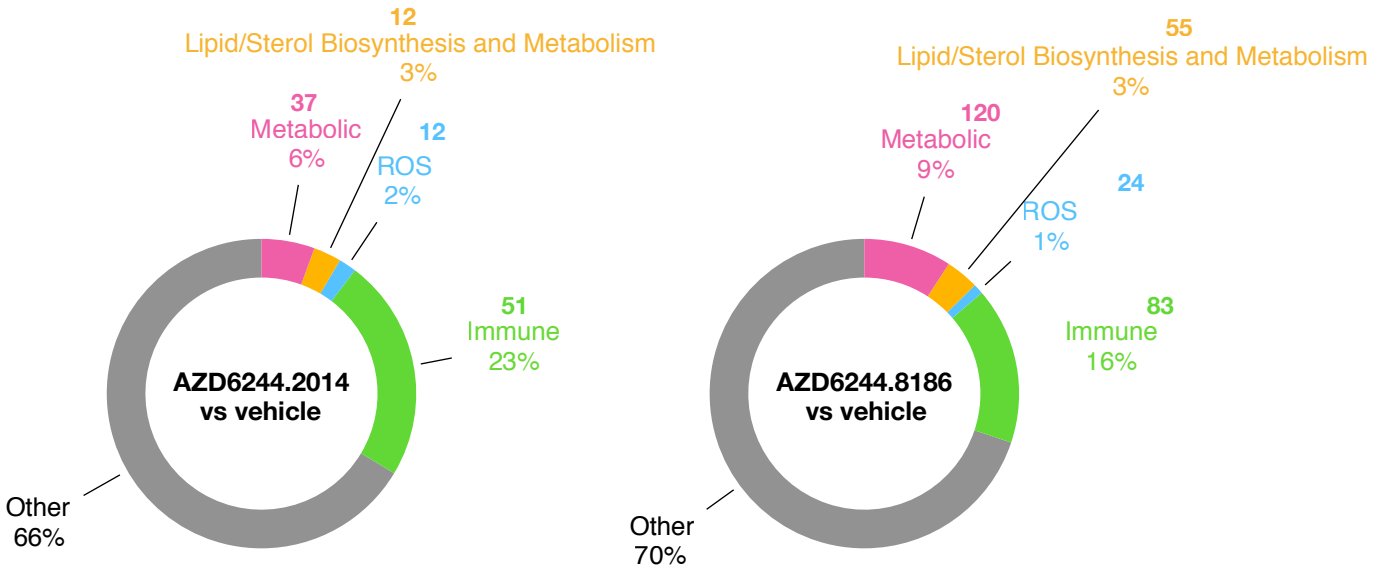


**Figure S1 | AZD6244.2014 and AZD6244.8186 enrich for metabolic and immune signature gene sets in AK CRC.** HGSEA data of AZD6244.2014 vs vehicle and AZD6244.8186 vs vehicle was sorted by highest to lowest log2fold enrichment to determine the gene sets most enriched in response to treatment in AK CRC mouse models **(A)** In AZD6244.2014 vs vehicle, the highest 10 enriched upregulated gene sets were dominantly metabolic; the highest 10 enriched down-regulated gene sets were dominantly immune signatures. Enrichment P.BH < 0.004, n=4. **(B)** In AZD6244.8186 vs vehicle, the highest 10 enriched upregulated gene sets had a wider range than AZD6244.2014 and were dominantly metabolic and lipid/ sterol biosynthesis and transport associated; the highest 10 enriched down-regulated gene sets were dominantly immune signatures similar to those of AZD6244.2014. Enrichment P.BH < 0.002, n=4. **(C)** In the AZD6244.2014 -treated models, metabolic and immune associated gene sets make up 6% and 23 % respectively and are controlled by 37 and 51 SDGs respectively. In the AZD6244.8186 -treated models, metabolic and immune gene sets make up 9% and 16% respectively and are controlled by 120 and 83 SDGs respectively. Enrichment P.BH < 0.004, n=4

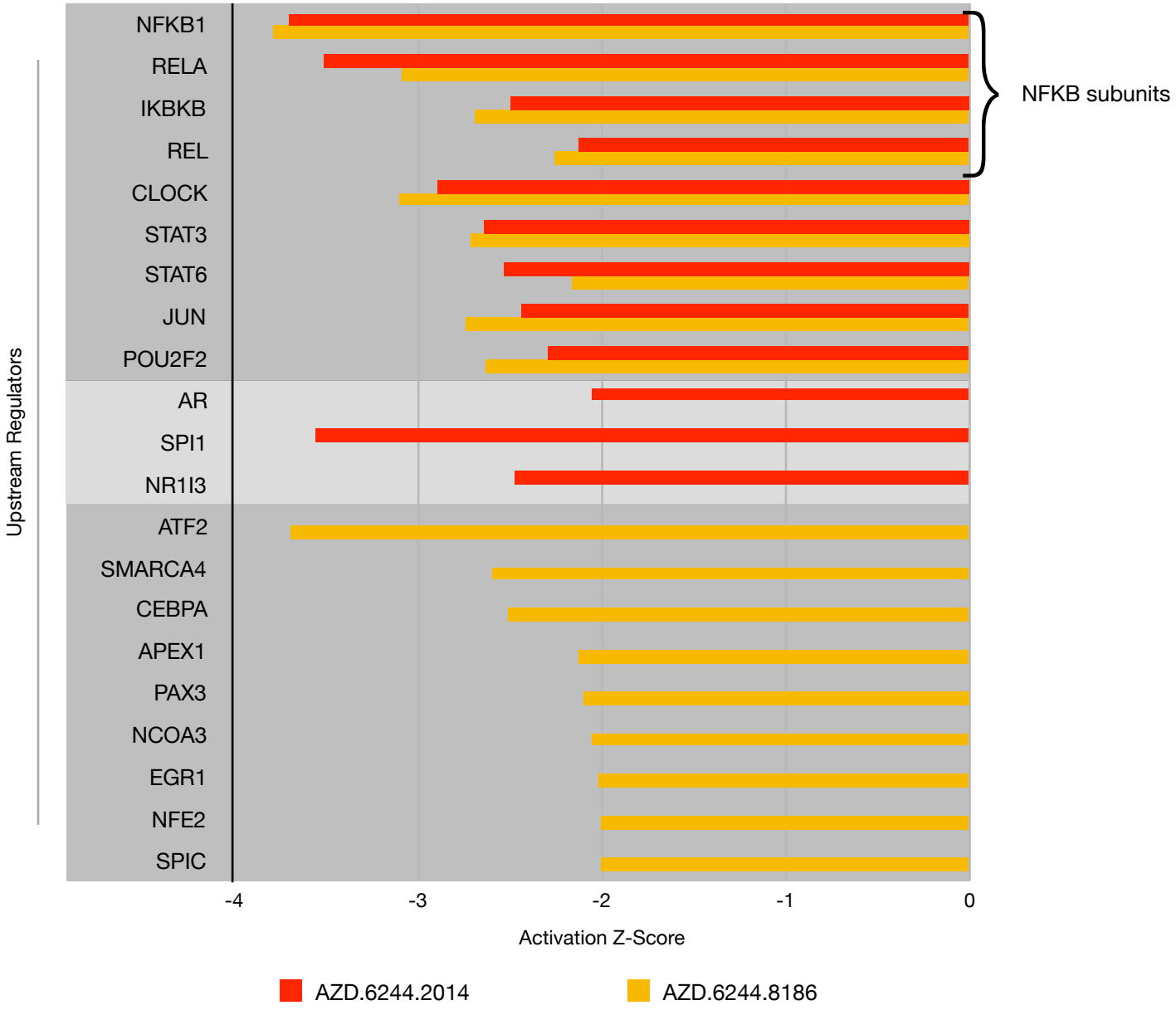


**Figure S2 | NFKB1 is the highest deactivated upstream regulator by AZD6244.2014 and AZD6244.8186.** The highest deactivated upstream regulators (absolute activation z-score > 2) for AZD6244.2014 in descending order are: NFKB1, SPI1, RELA. The highest deactivated upstream regulators (absolute activation z-score > 2) for AZD6244.8186 in descending order are: NFKB1, ATF2, CLOCK, RELA. Enrichment P.BH < 0.05, n=4.